Inositol Hexaphosphate (InsP6) Activates the HDAC1/3 Epigenetic Axis to Maintain Intestinal Barrier Function

Sujan Chetterjee [1], Loretta Viera- Preval [1], Zachary Sin [1], Nguyen Tran [1], Kevin Ritter [5], Xue Bessie Su[3], Jakob P. Centlivre [1], Saharat Jolak Ragsac[1], Richard Van[1, 2], Seungman Park [4], Mira V Han [1, 2], Qian Liu[1, 2], Brian P Hedlund[1], Adolfo Saiardi [3], Henning J. Jessen [5] and Prasun Guha[1,2,@]

[1]Nevada Institute of Personalized Medicine, University of Nevada, Las Vegas, NV, USA;

[2]School of Life Sciences, University of Nevada, Las Vegas, NV, USA,

[3]Medical Research Council Laboratory for Molecular Cell Biology, University College London, London, United Kingdom.

[4]Department of Mechanical Engineering, University of Nevada, Las Vegas, Las Vegas, NV, 89154, USA

[5] Institute of Organic Chemistry, Faculty of Chemistry and Pharmacy, University of Freiburg, Albertstr. 21, 79104 Freiburg, Germany

[@] Corresponding Author:

Prasun Guha, University of Nevada-Las Vegas, 4505 S Maryland Pkwy, Harry Reid Center, Rm 183C, Las Vegas, NV 89154, prasun.guha@unlv.edu, 702-895-2033

Abstract.

HDACs (histone deacetylase) play a crucial role in regulating gene expression, and the inhibition of these enzymes is gaining attention as a promising therapeutic approach for cancer treatment. Despite their significant physiological and clinical importance, the mechanisms of HDAC activation remain poorly understood. This study reveals that inositol polyphosphate multikinase (IPMK) is essential for activating HDAC1 and HDAC3 in cell lines and mice. *IPMK* deletion or inactivation of its kinase activity selectively impairs HDAC1/3's deacetylase activity, significantly influencing gene expression. Disruption of the IPMK-HDAC1/3 epigenetic axis results in transcriptional upregulation of matrix metalloproteinase (MMP) genes, exacerbating cell and intestinal permeability. Remarkably, treatment of *IPMK* KO cells with cell-permeable inositol hexaphosphate (InsP6) rescues these defects. This study elucidates the role of IPMK's kinase activity in HDAC1/3 activation and its implications for intestinal barrier function.

Introduction.

Epigenetic modifications allow mammalian cells to regulate gene expression without changing the genetic code [1, 2]. One classical epigenetic modification, histone acetylation (largely within nucleosome core histone N-terminal "tails"), strongly influences chromatin remodeling and gene expression[3,4]. Acetylation of histone lysine neutralizes the protein's positive charge, loosening interactions with negatively charged DNA phosphate groups, facilitating transcription factor binding to gene promoters/enhancers, and triggering transcription [5, 6]. Abnormal histone acetylation impacts the transcription of numerous genes, thereby influencing pathways such as cell adhesion [7], membrane permeability[8], oxidative stress[9], cell proliferation [10] , apoptosis [11,12] and inflammation [13,14].

Histone acetyltransferases (HATs) add acetyl groups to lysine residues[15], while histone deacetylases (HDACs) remove them[15]. Histone deacetylases (HDACs), particularly HDAC1 and 3, are key epigenetic regulators implicated in various diseases, including gastrointestinal disorders[16,17], and cancer [18,19]. Studies have shown that in mouse intestine, deletion of *HDAC1* or *HDAC3* leads to a Crohn's-like phenotype and increased intestinal permeability [16,20]. Aberrant HDAC3 expression or activation has been associated with poor prognosis in hepatocellular carcinoma[21] and B-cell lymphoma[22]. Notably, clinical trials using the HDAC1/3 selective inhibitor Entinostat have shown promising results in treating hormone receptor-positive, human epidermal growth factor receptor 2-negative (HR+/HER2-) advanced breast cancer [22] and additional phase-I trials are underway to evaluate its efficacy in treating solid tumors in adults and children[24]. Despite the significant physiological and clinical implications of HDACs, our

understanding of the signaling mechanisms regulating their enzymatic activity remains limited.

A HDAC3 crystal structure revealed the binding of the higher order inositol phosphate (HOIPs) InsP4 (inositol tetraphosphate) to HDAC3 facilitating its interaction with its co-repressor silencing mediator for retinoid and thyroid hormone receptors (SMRT) and nuclear receptor co-repressor 1 (NCOR1), thereby activating HDAC3's activity[25]. By contrast, SMRT and NCOR1 mutations that reduce InsP4 binding decrease HDAC3 activity in the mouse liver, affecting lipid metabolism[26]. Biochemical studies further identified high-affinity binding of another HOIP, InsP6, to both HDAC3 and HDAC1 *in vitro*[27]. However, it's unclear whether HOIPs play a pivotal role in influencing HDAC1/3-directed chromatin remodeling and gene expression influencing physiological functions.

The HOIP pathway involves a series of enzymes that sequentially add phosphates to the precursor InsP3, ultimately generating InsP4, InsP5, and InsP6. IPMK is the rate-limiting enzyme in the HOIP pathway, and deletion of *IPMK* diminishes intracellular concentration of InsP4, InsP5, and InsP6 [28]. Our study reveals that IPMK's inositol kinase activity is essential for HDAC1 and HDAC3's enzymatic activity, establishing an IPMK-HDAC1/3 epigenetic axis that regulates histone acetylation and global gene expression. Disruption of this axis leads to increased intestinal permeability in mice, a hallmark of Crohn's Disease[28,29]. Notably, mutations in IPMK have been identified as a marker for Crohn's Disease in GWAS and preclinical studies [30]. Overall, this research uncovers a novel IPMK-HDAC1/3 epigenetic mechanism linked to Crohn's-like phenotypes, particularly leaky gut syndrome, providing new insights into Crohn's disease pathogenesis and a potential therapeutic target.

Results

IPMK deletion in cell lines and mice intestinal epithelial cells (IECs) diminishes HDAC1 and HDAC3's enzymatic activity.

IPMK is the rate-limiting enzyme in the HOIP pathway that generates InsP4 and InsP5[28]. Previous studies indicated the potential role of HOIPs in activating HDAC3, a member of the class I HDAC family[27]. To test the effect of *IPMK* deletion in regulating class I HDAC activity, we created *IPMK* CRISPR KO HCT116 cells **(Extended Figure 1A, B).** We identified three clones with reduced HDAC3 activity, but the B09 clone showed the most significant loss **(Extended Figure 1C)**. Therefore, we used the B09 clone for further studies. To investigate the impact of IPMK loss of function on all Class I HDACs (comprised of HDAC1, 2, 3 and 8), we performed immuno-affinity purification of HDACs 1, 2, 3, and 8 from both wild-type (WT) and IPMK knockout (KO) HCT116 cells followed by an activity assay (Figure 1 A). IgG served as a negative control, and the fold change in HDAC activity was calculated relative to IgG in both IPMK wild-type (WT) and knockout (KO) samples. Interestingly, *IPMK* deletion selectively diminished HDAC1 and HDAC3's (HDAC1/3) enzymatic activity by 83.8% and 89.2% compared to WT without influencing others **(Figure 1 B).** This effect was confirmed in two additional *IPMK* CRISPR KO clones **(Extended Figure 1C),** with clone B09 exhibiting the most pronounced effect. Notably, *IPMK* deletion did not alter HDAC1/3 protein levels, which remained comparable to WT **(Figure 1 C)**. We chose the HCT116 intestinal epithelial cell line from colon cancer patients to CRISPR knock out *IPMK* because a previous study indicated maximum IPMK gene expression in the intestine[23]. Hence, using HCT116 cells would be instrumental to

determine the biological effect of *IPMK* loss. However, the finding in HCT116 was further confirmed in *IPMK* knock-out mouse embryonic fibroblasts (MEFs) cells, in which *IPMK* deletion markedly diminished HDAC1 and HDAC3's deacetylase activity **(Extended Figure 1D, E)**, demonstrating this effect is not limited to HCT116 cells only rather even preserved in mouse fibroblast cell lines.

We wonder whether IPMK loss of function *in vivo* mice model impairs HDAC1 and HDAC3's enzymatic activity. We used the Cre-lox approach to generate mice with intestinal epithelial cells (IECs) specifically lacking IPMK ($IPMK^{\Delta IEC}$). This was achieved by crossing IPMK-floxed mice ($IPMK^{F/F}$) with Villin-Cre driver mice, resulting in IPMK deficiency in IECs[30]. We flow purified IECs using FACS[31] and confirmed the purity (Extended **Figure 1 F-H).** Immuno-purification of HDAC1 and HDAC3 from primary IECs confirmed a 91.32% and 89.20% decrease in HDAC1 and HDAC3 activity in $IPMK^{\Delta IEC}$ mice **(Figure 1D, E)**. To address the potential confounding effects of long-term *IPMK* deletion on gut microbiome composition and its subsequent impact on HDAC1/3 activity in intestinal epithelial cells (IECs), we employed a Tamoxifen-inducible Villin Cre system for transient *IPMK* depletion. Strikingly, just 7 days of tamoxifen treatment resulted in significant IPMK protein depletion **(Figure 1 F)**, accompanied by a marked reduction in HDAC1/3 activity in mouse IECs **(Figure 1 G)**. This suggests that both long-term and transient *IPMK* loss of function leads to diminished HDAC1/3 activity in mouse IECs. Overall, the findings demonstrate that *IPMK* deletion selectively reduces HDAC1/3's enzymatic activity without affecting their protein expression, a phenomenon consistently observed across both cell lines and mouse IECs.

InsP6 treatment restored the enzymatic activity of HDAC1 and HDAC3 in *IPMK* KO cells.

The inositol kinase activity of IPMK, which generates InsP4 and InsP5 as precursors to InsP6 **(Figure 2 A)**, is highly conserved across species[28]. As expected, *IPMK* deletion in HCT116 cells markedly reduced InsP5 and InsP6 levels **(Extended Figure 2A)**. To explore whether IPMK's inositol kinase activity is critical for HDAC1 and HDAC3's enzymatic activity, we rescued *IPMK* KO *cells* (KO) with transient transfection of *WT-IPMK* or *Kinase-dead (KSA) IPMK.* Interestingly, rescuing *IPMK* KO cells with *WT-IPMK*, but not *KSA-IPMK*, restored HDAC1 **(Figure 2B)** and HDAC3's deacetylase activity **(Figure 2C-D).** This suggests that IPMK's kinase activity is crucial activating HDAC1 and HDAC3.

Next, we tried to restore HDAC1 and HDAC3's enzymatic activity with InsP4, InsP5, and InsP6 *in vitro* after immunopurification of HDAC1 and HDAC3 from *IPMK* KO cells. Biochemical analysis revealed that InsP6 rescued the enzymatic activity of HDAC1 and HDAC3 in a dose-dependent manner **(Figure 2E, F).** While 10 nM InsP6 [InsP (1,2,3,4,5,6) P6] restored around 50% of HDAC1 and HDAC3 activity (compared to 100% for WT), 1 μM InsP6 restored activity comparable to the WT-IPMK **(Figure 2E, F)**. Next, we explored the efficacy of other InsPs on rescuing HDAC1/3's enzymatic activity *in vitro* at 1 μM dose. Although InsP4 [InsP (1,4,5,6) P4] and InsP5 [InsP (1,3,4,5,6) P5] also restored HDAC1 and HDAC3 's activity at 1 μM **(Figure 2G, H),** restoration was less compared to InsP6. Further experiments revealed the exciting observation that a second InsP4 isomer [InsP (1,3,4,5) P4] and InsP3 [InsP (1,4,5) P3] failed to rescue HDAC1 and

HDAC3 activity, even at 10 μM **(Figure 2G, H)** dose, indicating that the 6th position phosphate is crucial for activating HDAC1 and HDAC3.

As IPMK is a physiological phospho inositide 3 kinase (PI3 kinase)[30] that also generates PIP3 (phospho inositide 3,4,5 triphosphate), we further tested the role of PIP3 in rescuing HDAC1 and HDAC3 activity when purified from *IPMK* KO cells. We found that even at 10 μM, PIP3 failed to restore HDAC1 and HDAC3 activity and was similar to the *IPMK* knockout **(Figure 2G, H)**. This indicates the crucial role of InsP4 [InsP (1,4,5,6) P4], InsP5, and InsP6 to activate HDAC1 and HDAC3, with InsP6 being the most effective.

IPMK directly binds to HDAC1/3.

We used an endogenous pull-down assay to examine the direct binding of IPMK to HDAC1/3 in *IPMK* wild-type (WT) and knockout (KO) cells **(Figure 3 A, B)**. As expected, immunoprecipitation (IP) of HDAC1 **(Figure 3 A)** and HDAC3 **(Figure 3 B)** from *IPMK WT* cells immunopurified endogenous IPMK, whereas IP from *IPMK KO* cells failed to do so. The data indicates endogenous IPMK interactions with HDAC1 and HDAC3. Further experiments are required to understand physical interaction of IPMK-HDAC1 and IPMK-HDAC3.

Loss of *IPMK* elevates histone acetylation.

As *IPMK* deletion diminishes HDAC1/3's deacetylase activity, we wondered whether loss of *IPMK* elevates histone acetylation. Western blot analysis of all acetylated histones **(Figure 4 A-B)** revealed a significant increase in H3K9, H3K18, H3K27, and H4K16

(Figure 4 A-B) acetylation in *IPMK* knockout HCT116 cells, with levels comparable to those observed in cells treated with the HDAC1/3-selective inhibitor Entinostat. Additionally, constitutive (*IPMK*$^{\Delta IEC}$) or tamoxifen-inducible loss of *IPMK* in mouse IECs (*IPMK* $^{Tam\text{-}\Delta IEC}$) also increased H3K9/27 and H4K16 acetylation compared to *IPMK*$^{F/F}$ mice **(Extended Figure 3 A- B)**. Interestingly, *IPMK* deletion did not affect the acetylase activity of P300 **(Extended Figure 3 C).** This finding confirms that the increased histone acetylation observed in *IPMK*-depleted cells and mouse models is a direct result of the loss of HDAC1/3 enzymatic activity and is independent of any potential gain of function of the protein acetyltransferase P300.

***IPMK* deletion induced transcriptional changes that resembled those seen with HDAC1/3 inhibition.**

Lysine acetylation of histone amino-terminal tails is a key regulator of transcription initiation[3]. Our bulk RNA-Seq analysis of *IPMK*-deleted HCT116 cells revealed significant transcriptional changes compared to wild-type cells, with 4014 genes upregulated and 3271 downregulated **(Figure 5 A)**. We compared these data to RNA-Seq results from HDAC1/3 inhibitor-Entinostat treated wild-type HCT116 cells **(Extended Figure 4A)** and found a strong positive correlation (Pearson correlation; R=0.90) between the transcriptomic changes in *IPMK* knockout cells and Entinostat-treated cells **(Figure 5 B)**. A significant overlap was observed, with 60.1% of upregulated genes **(Figure 5 C)** and 65.8% of downregulated genes **(Extended Figure 4B)** in *IPMK* KO cells also been up and down regulated in Entinostat-treated cells. These findings imply that more than 50% of gene regulation in *IPMK* knockout cells is likely to be mediated through the inhibition of HDAC1/3 activity. We termed this overlapping gene

set, the IPMK-HDAC-Overlap-Gene (IHOG). To validate these findings *in vivo*, we performed RNA-Seq analysis on intestinal epithelial cells (IECs) isolated from IPMK$^{\Delta IEC}$ and IPMK$^{F/F}$ mice **(Extended Figure 4 C)**. Notably, around 250 of upregulated genes **(Figure 5 D)** and 380 of downregulated genes **(Extended Figure 4D)** in IPMK$^{\Delta IEC}$ mice overlapped with the IHOG set, confirming the conservation of some transcriptional signatures in intact mouse intestines. Further analysis identified common functional pathways upregulated across *IPMK* knockout cells, Entinostat-treated wild-type cells, and *IPMK*-deficient intestinal epithelial cells from mice (IPMK$^{\Delta IEC}$). NOTCH1 signaling and the NABA ECM regulator pathway which includes the collagenase gene family, were consistently upregulated across these groups **(Figure 5 E)**. Given the association between IPMK and Crohn's disease and ulcerative colitis[30], we examined the expression of collagenase gene families in Crohn's disease patients from the Inflammatory Bowel Disease Transcriptome and Meta transcriptome Meta-Analysis (IBD TaMMA) database. Our results showed that multiple matrix metalloproteinases (MMPs) family genes were highly upregulated in human patient studies **(Figure 5 F)**.

Overall, this study suggests that the IPMK-HDAC1/3 epigenetic axis has a conserved influence on transcription from human cell lines to mouse models. Furthermore, the transcriptional alterations that promote the upregulation of collagenase gene families may lead to increased intestinal permeability [32].

Intestinal *IPMK* deletion associated with markedly increased cell and gut permeability.

Matrix metalloproteinases (MMPs) degrade extracellular matrix and disrupt cell adherent junctions, including tight junctions and desmosomes, thereby increasing cell permeability[33,32]. The upregulation of MMP is associated with compromised intestinal barrier function, leading to increased intestinal permeability and a "leaky gut" phenomenon, commonly observed in patients with Crohn's disease and ulcerative colitis[34]. Given these associations, we investigated the consequences of increased MMP production in *IPMK* knockout cells and mouse intestines on cell and intestinal permeability. To assess the impact of *IPMK* deletion on cell permeability, we employed a trans well assay using *IPMK WT* and *KO* HCT116 cells. We cultured these cells in a confluent layer on trans well insert and treated them with 4KD FITC-dextran **(Figure 6 A)**. Cell permeability will increase the leakage of 4KD FITC-Dextran from the upper cell inserts into the bottom chamber **(Figure 6 A)**. Spectrofluorometric analysis revealed that WT cells were not permeable before 20 minutes of 4KDa FITC-Dextran treatment, only showing penetration after this time point and reaching its a peak at 45-60 minutes **(Figure 6 B).** In contrast, *IPMK* knockout HCT116 cells exhibited a significant increase in FITC-dextran fluorescence after just 5 minutes, and reaching a maximum by 25 minutes **(Figure 6 B)**. Remarkably, this effect was completely blocked by pan-MMP inhibitor (Ilomastat) and cell-permeable InsP6 **(Figure 6 C)**). We further investigated the role of HDAC1/3 inhibition on cell permeability by pre-treating cells with Entinostat. Interestingly, Entinostat treatment to WT cells alone increased FITC fluorescence, an effect significantly attenuated when combined with the pan-MMP inhibitor Ilomastat **(Figure 6 C)**. DAPI and crystal violet staining followed by spectroscopic analysis ruled out cell number variations as a potential artifact **(Extended Figure 5 A, B)**. These findings

indicate that *IPMK* deletion and HDAC1/3 inhibition increase cell permeability, likely through a shared mechanism involving MMP upregulation.

In vivo studies further supported these findings. We orally gavaged mice with FITC-dextran (4KD) and found that IPMK$^{\Delta IEC}$ and tamoxifen-inducible IPMK $^{Tam\text{-}\Delta IEC}$ mice exhibited significantly elevated serum concentrations of FITC-dextran compared to IPMK$^{F/F}$ mice **(Figure 6D-F)**. This discovery indicates that long-term deletion of *IPMK* in mouse intestinal epithelial cells (IECs) or transient loss following tamoxifen treatment both leads to increased intestinal permeability. Collectively, the data implicate a potential mechanistic link between IPMK, MMPs, and HDAC1/3 activity, suggesting that *IPMK* depletion elevates MMP activity, thereby compromising intestinal barrier integrity.

Discussion

The crystal structure of HDAC3 revealed InsP4 as a molecular bridge linking HDAC3 to its co-repressors[25]. This finding suggests that higher-order inositol phosphates (HOIPs) may play a crucial role in regulating cellular epigenetic changes[25,27,35]. Herein, we identified InsP6 as a crucial activator of the HDAC1/3-epigenetic axis influencing histone acetylation and gene expression. Since IPMK is the rate-limiting enzyme in HOIP biosynthesis[28], its deletion markedly diminishes InsP4, InsP5, and InsP6 levels in intact animal tissue and cell lines[28]. Our study uncovered that *IPMK* deletion **(Figure 1A-G, Extended Figure 1A-H)** or loss of its inositol kinase activity **(Figure 2 A-D, Extended Figure 2 A)** selectively diminished HDAC1 and HDAC3's deacetylase activity in cell lines and mouse intestines**.** The loss of HDAC1/3's enzymatic activity in *IPMK* KO cells was successfully rescued by InsP6 treatment **(Figure 2 E-H)**, demonstrating its function as a potent HDAC1 and HDAC3 activator. While *IPMK* loss significantly increases histone acetylation **(Figure 4, Extended Figure 3)**, bulk RNA-seq analysis showed that around half of the regulated genes in *IPMK* knockout HCT116 cells are likely due to the inhibition of HDAC1/3's enzymatic activity **(Figure 5C, Extended Figure 4B)**. Notably, the significant number of genes identified in cell lines regulated by the IPMK-HDAC1/3 epigenetic axis was found to be conserved in IPMK$^{\Delta IEC}$ mice **(Figure 5D, Extended Figure 4D)**, underscoring the significance of this epigenetic axis in regulating transcription across cell lines and animal models.

Next, we explored the physiological implications of the IPMK-HDAC1/3 epigenetic axis. Transcriptomic analysis revealed that disruption of the IPMK-HDAC1/3 axis resulted in the hyper-transcription of matrix metalloproteinase (MMP)-related genes. This finding is

particularly relevant to Crohn's disease, where several MMP genes are transcriptionally upregulated in intestinal epithelial cells (IECs) **(Figure 5 F)**. The enhanced MMP production leads to the proteolytic digestion of tight junctions[36], thereby compromising cell-cell adhesion and elevating intestinal permeability which potentially contributes to the progression of Crohn's. Indeed, *IPMK* deletion led to increased cell permeability in both *in vitro* tissue culture experiments **(Figure 6 A, B)** and *in vivo* mouse models, with intestinal-specific *IPMK* deletion significantly enhanced gut permeability **(Figure 6 D)**. Remarkably, we found that cell permeable InsP6 treatment prevents cell permeability **(Figure 6C).** Previous research suggested the intriguing possibility of gut microbiota-derived inositol phosphates, particularly InsP3, activating HDAC3 in the intestine [37]. However, our current study identifies InsP6 as the most potent inducer of HDAC3 and HDAC1 **(Figure 2 E-H)**, which markedly prevents cell permeability in *IPMK* knockout cells **(Figure 6C)**. InsP6, also known as phytic acid, is abundant in plant-based diets, although its low bioavailability poses a challenge for therapeutic use[38]. Consequently, enhancing InsP6 bioavailability through chemical modification holds promise as an HDAC1/3 activator, offering a means to finely regulate the epigenetic landscape of cells. This approach could potentially contribute to therapeutic interventions in various diseases, including Crohn’s disease and ulcerative colitis, by modulating the IPMK-HDAC1/3 epigenetic axis.

Materials and Methods.

Cell culture and Entinostat treatment.

Human Colon Tumor 116 (HCT116) and Mouse Embryonic Fibroblast (MEF) cells were cultured in McCoy's 5A medium or Dulbecco's Modified Eagle's Medium (DMEM) respectively. DMEM media was supplemented with 10% FBS, 2 mM L-glutamine, 100 U/mL penicillin, and 100 mg/mL streptomycin was used for MEF cells. While McCoy's 5A medium was supplemented with 10% FBS, 100 U/mL penicillin, and 100 mg/mL streptomycin. *IPMK* wild-type (WT) and knockout (KO) HCT116 cells were generated using CRISPR/Cas9 technology, which partially deleted exon 5 and the coding region of exon 6. Afterward, clonal populations were isolated, purified, and screened for IPMK expression.

For the generation of *IPMK* KO MEF cells, floxed MEFs were immortalized through transfection with pSG5-Large T (a plasmid provided by William Hahn to Addgene) using the Polyfect transfection reagent (Qiagen) according to the manufacturer's instructions. After serial passaging five times to select against non-transformed cells, *IPMK* KO cells were produced by transducing floxed cells with an adenovirus carrying the Cre recombinase gene (obtained from the University of Iowa Gene Transfer Vector Core). The virus was combined with Gene Jammer (Stratagene) transfection reagent to improve transduction efficiency. Clonal populations were then purified and screened for IPMK expression[30].

Entinostat treatment.

IPMK-WT HCT 116 cells were then treated with Entinostat MS-275 (5 μM) (Selleckchem.com Cat# S1053) for 8 hours followed by estimation of histone acetylation by immunoblot analysis and purified RNA for sequencing.

Animals.

All protocols were approved by the Institutional Animal Care and Use Committee (IACUC), University of Nevada, Las Vegas. Mice were housed according to institutional guidelines, in a controlled environment at a temperature of 22_C ± 1_C, under a 12-h dark-light period and provided with standard chow diet and water *ad libitum*. Male and female *IPMK* $^{F/F}$, *IPMK*$^{\Delta IEC}$ or *IPMK* $^{Tam\text{-}\Delta IEC}$ (between eight to 16 weeks) were used. Specifically, intestinal epithelial cells from male mice were used for biochemical and transcriptomic analysis. All mice were maintained in 129SV-C57BL/6 mixed background.

Generation of intestine specific *IPMK* knock out mice.

Ipmk $^{F/F}$ mice were generated as previously described. *Ipmk*$^{F/F}$ mice were crossed with C57BL/6J mice carrying Cre expressed under the control of the murine villin promoter as described previously to create intestinal-specific *Ipmk* knockout mice (*Ipmk*$^{\Delta IEC}$). Homozygous *Ipmk*$^{F/F}$ mice were crossed with the *Ipmk*$^{\Delta IEC}$ mice, which mediate excision of floxed alleles in the intestine. All mice were maintained on a C57BL/6J background and were 10th generation backcrossed. Mice were housed in a 12-hour light/12-hour dark cycle at 22°C and fed standard rodent chow. All research involving mice was approved

by University of Nevada, Las Vegas's Institutional Animal Care and Use Committee (IACUC) [30].

Tamoxifen treatment.

To generate intestinal epithelial cell specific transient IPMK deleted mice model. *IPMK* exon 6 was excised by tamoxifen (SIGMA Cat no. #T5648-1G) dissolved in Olive oil (SIGMA Cat no. #O1514-500ml) at a concentration of 10 mg ml^{-1} and 200 µl /25 gm body weight once a day injected interperitoneally for seven days. Control mice received equal volume of tamoxifen. Intestinal epithelial cells were harvested after six days of recovery[39].

Generation of IPMK antibody:

Custom anti-IPMK antibody was generated in collaboration with Pro-Sci. The anti-rabbit IPMK antibody had been raised against IPMK amino acids 295–311 (SKAYSRHRKLYAKKHQS). The antibody recognizes mouse and human IPMK.

Western Blot analysis.

Cell lysates were prepared through syringe flush by using a salt-free (NaCl-free) Lysis buffer (50 mM Tris pH 7.5, 50 mM potassium acetate, 5 % v/v glycerol, 0.3 % v/v Triton X-100, one tablet of Roche complete protease inhibitor). We used salt-free (NaCl-free) lysis buffer for all the assays because high salt concentration dissociates higher-order inositol phosphate (HOIPs) from HDAC1/3, which is essential for their deacetylase activity[25,27]. Samples were centrifuged at 15,000 g for 10 min, and the protein

concentration of the supernatant was measured. Proteins were resolved by SDS-polyacrylamide gel electrophoresis (NuPAGE Bis-Tris Midi GEL, Life Technologies, Cat #: WG1402BX10) and transferred to Immobilion-P PVDF (Millipore-Sigma, Cat #: IPVH00010) transfer membranes. The membranes were incubated with primary antibody diluted in 3% BSA in Tris- Buffered Saline with Tween 20 (20 mM Tris-HCl, pH 7.4, 150 mM NaCl, and 0.02% Tween 20) overnight incubation at 4°C. Respective antibodies for western blot anti-HDAC3 (Santa Cruz Biotechnology, Cat #: sc-376957), anti-HDAC1 (Santa Cruz Biotechnology, Cat #: sc-81598), anti-HDAC2 (Santa Cruz Biotechnology, Cat #: SC-7899), anti-HDAC8 (Biolegend, Cat #: 685504), IPMK (Generated in our lab) anti-beta actin (ProteinTech, Cat #: 81115-1-RR), anti-lamin (ProteinTech, Cat #: 12987-1-AP), anti-SMRT (Bethyl Laboratories, Cat #: A301-148A), anti-Ncor1 (Cell Signaling Technology, Cat #: 5948), anti-Rcor1 (ProteinTech, Cat #: 26686-1-AP), Sin3A (ProteinTech, Cat #: 14638-1-AP), anti-DNTTIP1 (Bethyl Laboratories, Cat #: A304-048A), anti-H3 (Cell Signaling Technology, Cat #: 12648), anti-H3k8Ac (Cell Signaling Technology, Cat #: 2598), anti-H3k9Ac (Cell Signaling Technology, Cat #: 9649), anti-H3k18Ac (Cell Signaling Technology, Cat #: 13998), anti-H3k27Ac (Abcam, Cat #: ab4729) ,anti-H3k56Ac (Cell Signaling Technology, Cat #: 4243), anti-H4k8Ac (Cell Signaling Technology, Cat #: 2594), anti-H4k12Ac (Cell Signaling Technology, Cat #: 13944), anti-H4k16Ac (Cell signaling Technology, Cat #: 13534S) and anti-Myc (Invitrogen, Cat #:46-0709). Following primary antibody incubation, the PVDF membrane was washed three times with TRIS-buffered saline/Tween-20, and incubated with HRP-conjugated secondary antibody (ECL, Cat #s: NA934V and NA931V), and the bands visualized by chemiluminescence (Super Signal West Pico, Pierce, Cat #: 34579). The

depicted blots are representative replicates selected from at least three experiments. Densitometric analysis was performed using Image J software. Blots for acetylated histones were stripped using Restore Western Blot stripping buffer (Thermo Scientific, Cat # 21059), then reprobed with H3 antibody (Cell Signaling Technology, Cat #: 12648S) at room temperature for 2 h followed by secondary antibody incubation and development.

HDAC (histone deacetylase) activity.

To analyze deacetylase activity of specific Class I HDAC members, the HDAC1, 2, 3 and 8 were individually immuno-purified, followed by an activity assay using the following kits: HDAC Assay Kit (Active Motif, Cat#: 56200 for HDAC1, 2 and 8) and the HDAC3 Assay Kit (BPS, Cat#: 10186-628). Since high salt concentration dissociates higher-order inositol phosphates (HOIPs) from HDAC1/3, which are crucial for their deacetylase activity, WT and IPMK-KO HCT 116 cells were lysed in salt-free (NaCl-free) lysis buffer (50 mM Tris pH 7.5, 50 mM potassium acetate, 5 % v/v glycerol, 0.3 % v/v Triton X-100, one tablet of Roche complete protease inhibitor) [25,27,35]. Then, the lysate was centrifuged at 15,000 g for 10 min, and the protein concentration of the supernatant was measured. Equal amount, around 20 µg total protein from the lysate was incubated against anti-HDAC1 (Santa Cruz Biotechnology, Cat # sc-81598), anti-HDAC2 (Santa Cruz Biotechnology, Cat #: sc-7899), anti-HDAC3 (Santa Cruz Biotechnology, Cat #: sc-81600) and anti-HDAC8 (Biolegend, Cat #: 685504) antibodies, respectively, at 4°C for 1 hour followed by capturing antibody with EZview A/G beads (Millipore Sigma, Cat #: E3403). Beads were washed 3x with an ice-cold reaction buffer (supplied with the kit). After a specific substrate reaction, fluorescence was measured using a Spectra max iD5 plate

reader (Molecular Devices). All measurements were performed in triplicate, and data was analyzed using GraphPad Prism (version 6.0, GraphPad Software, Inc) [25,27].

HAT (histone acetyl transferase activity).

HAT activity was measured by following the HAT Assay Kit (Abcam, Cat #: ab-204709) protocol. WT and IPMK-KO HCT 116 cells were lysed in salt-free (NaCl-free) lysis buffer (50 mM Tris pH 7.5, 50 mM potassium acetate, 5 % v/v glycerol, 0.3 % v/v Triton X-100, Roche complete protease inhibitor)[25,27,35]. Samples were centrifuged at 15,000 g for 10 min, and the protein concentration of the supernatant was measured. Equal amount around 20 µg total protein from the lysate was incubated against anti-p300 CBP HAT antibody (Cell Signaling Technology, Cat #: 86377) respectively at 4°C for 90 min, followed by capturing the antibody with EZview A/G beads (Millipore-Sigma, Cat #: E3403). Beads were washed 3x with an ice-cold reaction buffer (supplied with kit). Immunoprecipitated P300 was used as a protein source. Absorbance was measured after specific substrate reaction by using a Spectramax iD5 plate reader (Molecular Devices). All measurements were performed in triplicate and data analyzed using GraphPad Prism (version 6.0, GraphPad Software, Inc).

Intestinal Epithelial cell purification.

The ileum (similar length as colon moving proximal from the ileocecal junction), cecum and colon were dissected from mice. After five time washing with ice cold PBS, the tissues were opened longitudinally and cut into small fragments (2–3 cm in length). To prepare single cell suspension after washing three time with PBS, small intestinal fragments were

incubated in 30 mM EDTA-PBS on ice for 30 min, during which the tissues were shaken vigorously every 5 min. Isolated crypts were washed once with cold PBS and dissociated using TrypLE Express (Invitrogen Cat# 12604021) for 10 min at room temperature. Cell suspensions were passed through a 70-mm cell strainer and then labeled with a cocktail of fluorescent antibodies specific for APC-CD45 (BioLegend, Cat# 103113), FITC-CD31 (BioLegend, Cat# 102406), PE/Cy7-TER-119 (BioLegend, Cat# 116222), and PE-EpCAM (Thermo Fisher Scientific, Cat# 12-5791-83). Dead cells were excluded using Tail Cell Cycle Solution (Invitrogen, Cat# A10798). $CD45^{-}CD31^{-}$ $TER\text{-}119^{-}$ EpCAM+ ECs were sorted using a SONY SH800S Cell Sorter[31].

InsP6 Rescuing HDAC1 activity.

WT and *IPMK*-KO HCT116 cells were lysed in salt-free (NaCl-free) lysis buffer (50 mM Tris pH 7.5, 50 mM potassium acetate, 5 % v/v glycerol, 0.3 % v/v Triton X-100, and one Roche complete protease inhibitor tablet)[25,27,35]. Samples were centrifuged at 15,000 g for 10 min, and the protein concentration of the supernatant was measured. Equal amount, 20 µg total protein from the lysate was incubated against anti-HDAC1 antibodies respectively at 4°C for 1 hr, followed by capturing antibodies with EZview A/G beads (Millipore Sigma, Cat #: E3403). Beads were washed 3x with an ice-cold reaction buffer (supplied with the kit). Following washing, beads were resuspended in reaction buffer then beads were incubated with 1nM, 10nM, 100nM, 500nM, 1µM, 5µM and 10µM concentrations of InsP6 (Sigma Aldrich Cat #: P8810-100G) for 1 hr at room temperature. After incubation, beads were washed 3x with reaction buffer. HDAC1 activity was measured by the addition of a fluorogenic substrate provided by the HDAC1 Assay Kit

(Active Motif, Cat#: 56200) and read using a Spectramax iD5 plate reader (Molecular Devices). All measurements were performed in triplicate data and analyzed using GraphPad Prism (version 6.0, GraphPad Software, Inc)[25,27,35].

InsP6 Rescuing HDAC3 activity.

WT and *IPMK*-KO HCT116 cells were lysed in salt-free (NaCl-free) lysis buffer (50 mM Tris pH 7.5, 50 mM potassium acetate, 5 % v/v glycerol, 0.3 % v/v Triton X-100, and one Roche complete protease inhibitor tablet)[25,27,35]. Samples were centrifuged at 15,000 g for 10 min, and the protein concentration of the supernatant was measured. Equal amount, 20 µg total protein from the lysate was incubated against anti-HDAC3 antibodies respectively at 4°C for 1 hr, followed by capturing antibodies with EZview A/G beads (Millipore Sigma, Cat #: E3403). Beads were washed 3x with an ice-cold reaction buffer (supplied with the kit). Following washing, beads were resuspended in reaction buffer then beads were incubated with 1nM, 10nM, 100nM, 500nM, 1µM, 5µM and 10µM concentrations of InsP6 (Sigma Aldrich Cat #: P8810-100G) for 1 hr at room temperature. After incubation, beads were washed 3x with reaction buffer. HDAC3 activity was measured by the addition of a fluorogenic substrate provided by the HDAC Assay Kit (BPS, Cat #: 10186-628) and read using a Spectramax iD5 plate reader (Molecular Devices). All measurements were performed in triplicate data and analyzed using GraphPad Prism (version 6.0, GraphPad Software, Inc)[25,27,35].

Analysis of rescuing HDAC1 activity using PIP3, InsP3, Ins (1,3,4,5)P4, Ins(1,4,5,6)P4, InsP5 and InsP6.

WT and *IPMK*-KO HCT116 cells were lysed in salt-free (NaCl-free) lysis buffer (50 mM Tris pH 7.5, 50 mM potassium acetate, 5 % v/v glycerol, 0.3 % v/v Triton X-100, and one Roche complete protease inhibitor tablet)[25,27,35]. Samples were centrifuged at 15,000 g for 10 min, and the protein concentration of the supernatant was measured. Equal amount, 20 µg total protein from the lysate was incubated against anti-HDAC1 antibodies respectively at 4°C for 1 hr, followed by capturing antibodies with EZview A/G beads (Millipore Sigma, Cat #: E3403). Beads were washed 3x with an ice-cold reaction buffer (supplied with the kit). Following washing, beads were resuspended in reaction buffer then beads were incubated with either 10µM concentration of PIP3, InsP3, Ins(1,3,4,5)P4 or 1µM Ins(1,4,5,6)P4, InsP5 and InsP6 (Sigma Aldrich Cat #: P8810-100G) for 1 hr at room temperature. After incubation, beads were washed 3x with reaction buffer. HDAC1 activity was measured by the addition of a fluorogenic substrate provided by the HDAC Assay Kit (Active Motif, Cat#: 56200) and read using a Spectramax iD5 plate reader (Molecular Devices). All measurements were performed in triplicate data and analyzed using GraphPad Prism (version 6.0, GraphPad Software, Inc)[25,27].

Analysis of rescuing HDAC3 activity using PIP3, InsP3, Ins (1,3,4,5) P4, Ins(1,4,5,6)P4, InsP5 and InsP6:

WT and *IPMK*-KO HCT116 cells were lysed in salt-free (NaCl-free) lysis buffer (50 mM Tris pH 7.5, 50 mM potassium acetate, 5 % v/v glycerol, 0.3 % v/v Triton X-100, and one Roche complete protease inhibitor tablet). Samples were centrifuged at 15,000 g for 10 min, and the protein concentration of the supernatant was measured. Equal amount, 20 µg total protein from the lysate was incubated against anti-HDAC3 antibodies respectively

at 4°C for 1 hr, followed by capturing antibodies with EZview A/G beads (Millipore Sigma, Cat #: E3403). Beads were washed 3x with an ice-cold reaction buffer (supplied with the kit). Following washing, beads were resuspended in reaction buffer then beads were incubated with either 10μM concentration of PIP3, InsP3, Ins(1,3,4,5)P4 or 1μM Ins(1,4,5,6)P4, InsP5 and InsP6 (Sigma Aldrich Cat #: P8810-100G) for 1 hr at room temperature. After incubation, beads were washed 3x with a reaction buffer. HDAC3 activity was measured by the addition of a fluorogenic substrate provided by the HDAC3 Assay Kit (BPS, Cat #: 10186-628) and read using a Spectramax iD5 plate reader (Molecular Devices). All measurements were performed in triplicate data and analyzed using GraphPad Prism (version 6.0, GraphPad Software, Inc)[25,27].

Plasmids and Recombinant Proteins.

pMX-myc, pMX-*IPMK*-*WT*-myc and pMX-*IPMK*-*KSA*-myc plasmids transiently transfected into *IPMK*-KO HCT 116 cells using Lipofectamine 3000 (Cat no. L3000001, Thermo Scientific) according to the manufacturer protocol. Recombinant myc-IPMK was purchased from Origene, (Cat #: TP309343) while recombinant GST-HDAC1 (Cat #: H83-30G), GST-HDAC3 (Cat #: H85-30G) and GST (Cat #: G52-30U) were purchased from Signal Chem.

Immunoprecipitation.

To analyze endogenous binding, HCT116 cells were lysed in salt-free lysis buffer (50 mM Tris pH 7.5, 50 mM potassium acetate, 5 % v/v glycerol, 0.3 % v/v Triton X-100, and one Roche complete protease inhibitor tablet). For the endogenous immunoprecipitation (IP), respective antibodies against HDAC1 or HDAC3 were used, followed by western blot of

the binding partners. In brief, the IP was performed from 500 ug of protein lysate. Protein lysates were incubated for 2 hr at 4°C with respective antibodies, then the antibody-protein complex was captured with EZview A/G beads (Millipore Sigma, Cat #: E3403). Beads were pelleted and washed with lysis buffer 3x, followed by elution in sample buffer. Immunoprecipitated samples were resolved on a NuPAGE Bis-Tris gel, followed by western blotting.

***In vitro* Binding assay.**

Equal amount of recombinant myc-IPMK (Origene, Cat #: TP309343) was co-incubated with either recombinant GST-HDAC1 (Signal Chem, Cat #: H83-30G), GST-HDAC3 (Signal Chem, Cat #: H85-30G) or GST (Signal Chem, Cat #: G52-30U) in lysis buffer and the complex was maintained for 30 min at 4°C. After the addition of GST beads, incubation continued for an additional 45 min and washed 3x with ice cold lysis buffer. SDS sample buffer was added and binding was confirmed by western blotting of anti-Myc antibodies[28].

Trans well assay.

Trans well filter inserts (pore size 1.0 µm, 12 mm diameter, polyester membrane, Corning, New York, USA) were coated with fibronectin (10 µg/ml; Sigma) used as insert for 24 well plate. For time dependent permeability assay WT and *IPMK*-KO HCT116 cells were seeded (0.25×10^6 cells/well) and grown on transwell filters for 48 hours until reaching confluency. FITC-dextran 4 kDa-FITC-Dextran (Sigma-Aldrich, Cat no: #FD4-1G) was added to the top well at 25 mg/ml. at 37°C, and fluorescence was measured after 0 min,

5 min, 10 min, 15 min, 20 min, 25 min, 30 min, 45 min and 1 hr. Using a Spectramax iD5 plate reader (Molecular Devices, (excitation 485 nm/emission 535 nm[40].

To analyze crucially of IPMK or InsP6 in cell permeability, WT and *IPMK*-KO HCT116 cells were seeded (0.25 × 10^6 cells/well) and grown on trans well filters for 48 hours until reaching confluency. Confluent monolayers of WT and *IPMK*-KO HCT 116 cells were treated with similar amounts of PBS (as a negative control), Entinostat (5μM), Ilomastat (10μM) [41] or cell permeable InsP6 (50μM) [42,43] overnight. FITC-dextran 4 kDa-FITC-Dextran (Sigma-Aldrich, Cat no: #FD4-1G) was added to the top well at 25 mg/ml for 20 min at 37°C, and fluorescence was measured using a Spectramax iD5 plate reader (Molecular Devices, (excitation 485 nm/emission 535 nm)[44].

To analyze cell number variation in the reaction plate, after the experiment, cells with transwell inserts were gently washed thrice with PBS and were fixed with 4 % paraformaldehyde followed by staining with either DAPI or Crystal violet respectively. For DAPI, after 5 min incubation with DAPI solution and three times washed with PBS fluorescence was measured at 358 nm-461 nm[45]. For Crystal Violet staining, cells were 10 min stained with 100μL 2% crystal violet solution and washed six times with PBS. The stained cells were then treated with 350 μL of lysing solution (prepared by mixing 100 mL of 5.88% Sodium Citrate solution with 100 mL of 50% Ethanol and adjusting the pH to 4.2 with HCl) for 30 minutes while gently shaking on a rocking shaker. Following this, 60 μL of the lysate was diluted in 240 μL of dH2O, and absorbance was measured at 590 nm.

FITC dextran intestinal permeability assay.

IPMK$^{F/F}$ and either IPMK$^{\Delta IEC}$ or IPMK$^{\Delta Tam\text{-}IEC}$ mice were fasted for 4 hours with access to water before being gavaged with 4 kDa-FITC-Dextran (Sigma-Aldrich, Cat no: #FD4-1G) at a single dose of 0.6mg/gm body weight. Untreated control group received equal amount of PBS. Fluorescence intensity of plasma samples was measured (excitation 485 nm/emission 535 nm) after 4 hours of gavage. Value was represented as a fold change in respect with untreated control group after blank subtraction. All measurements were performed using GraphPad Prism (version 6.0, GraphPad Software, Inc)[46].

Intracellular inositol content analysis using HPLC:

IPMK-WT and *KO* HCT116 cells were plated at a density of 250,000 cells per 60 mm plate, then labeled with 60 mCi (1 Ci = 37 GBq) [3H] myo-inositol (PerkinElmer) in conventional cell culture media for three days. To extract soluble inositol phosphates, cell pellets were suspended in 300 mL of ice-cold 0.6 M perchloric acid buffer (0.1 mg/mL IP6, 2 mM EDTA) and incubated on ice for 1 min. Ninety mL of 1 M potassium carbonate with 5 mM EDTA were added and incubated on ice for 1 h. Extracts were centrifuged at 12,000 rpm for 15 min. The supernatant was collected and analyzed by HPLC using a Partisphere SAX column (Whatman Inc.). The column was eluted with a gradient generated by mixing Buffer A (1 mM EDTA) and Buffer B (Buffer A plus 1.3 M (NH4)2HPO4, pH 3.8 with H3PO4). The 1 mL fractions were collected and counted using 5 mL of Ultima-Flo AP mixture (PerkinElmer)[47].

RNA isolation and library preparation.

Total RNA from was isolated by using RNAeasy Mini Kit (Qiagen Cat no.74104) by following manufacturer kit protocol. For RNA-seq, libraries were prepared from total RNA by using True Seq RNA Library Prep Kit V2 (Illumina).

RNA seq analysis.

FASTQ files were retrieved from sequencing. All pre-alignment and post-alignment QA/QC and data analysis were performed in partek (v.12.0.0). Reads were aligned to the whole genome using hg19 assembly with STAR (v.2.7.8a). Aligned reads were quantified to hg19 annotation model using HTSeq (v.0.11.0). Differential analysis was performed for IPMK knockout versus wild-type using DESeq2 (v.3.5) [48,49].

Pathway analysis.

Pathway analysis was performed on significantly upregulated genes (FDR <= 0.05 and log2FoldChange >= 2) using Metascape (v.3.5). These genes were queried against KEGG Pathway, Reactome Gene Sets, Canonical Pathways, and WikiPathways using the custom analysis tool. Terms with a p-value < 0.01, a minimum count of 3, and an enrichment factor > 1.5 were considered. All genes were used as background gene list[49].

Pearson correlation analysis.

Correlation of gene expression changes between *IPMK*-deleted HCT116 cells and 5 μM Entinostat-treated wild-type HCT116 cells was calculated using Pearson correlation

coefficient. The Pearson correlation was calculated using the COR function in R (v.4.3.2), with the method parameter set to “Pearson”.

Statistical analysis.

All plots and statistical analyses were performed with Prism 9 (GraphPad) software. Statistical significance was determined by either Student’s t-test (two-tailed) for two groups or 1-way ANOVA for multiple groups with similar samples. Error bars represent the standard deviation of the mean and indicate replicates or the number of animals employed. Results were representative of at least three independent experiments (n). Differences between groups were considered significant when *$p<0.01$, **$p<0.001$, and ***$p<0.0001$. Graphs were generated by using either Prism 9 (GraphPad) software or R software.

Acknowledgements:

This work was supported by NIH 5P20GM121325 COBRE grant and University of Nevada, Las Vegas start-up funds to Prasun Guha. This work was supported by UK Research and Innovation (UKRI)'s Medical Research Council (MRC) grant MR/T028904/1. We like to thank NIPM's Genomic core for assisting with instruments and experiments.

Competing interests:

The authors declare no conflict of interests. All authors reviewed the results and approved the final version of the manuscript.

Author Contributions:

PG conceived the study. PG and SC designed the experiments. SC performed most experiments. LVP validated major biochemical experiments. SC performed wet lab experiments related to NGS studies. ZS and LVP performed most of the NGS data analysis. KR and HJJ generated the cell permeable InsP6. XBS and AS analyzed intercellular inositol content. NT performed biochemical experiments. JC and BH did sequencing data analysis. QL performed NGS data validation. SJR maintained animal colony and isolate animal samples for genotyping. RV and MVH analyzed NGS data. SP performed mathematical analysis of transwell assay. SC and ZS designed the Figures. PG, and SC wrote the manuscript.

References:

1. Gibney ER, Nolan CM. Epigenetics and gene expression. *Heredity (Edinb)*. 2010;105(1):4–13. doi: 10.1038/hdy.2010.54.

2. Feinberg AP. Phenotypic plasticity and the epigenetics of human disease. *Nature*. 2007;447(7143):433–440. doi: 10.1038/nature05919.

3. Morales V, Richard-Foy H. Role of histone N-terminal tails and their acetylation in nucleosome dynamics. *Mol Cell Biol*. 2000;20(19):7230–7237. doi: 10.1128/MCB.20.19.7230-7237.2000.

4. Gallinari P, Di Marco S, Jones P, Pallaoro M, Steinkuhler C. HDACs, histone deacetylation and gene transcription: From molecular biology to cancer therapeutics. *Cell Res*. 2007;17(3):195–211. doi: 10.1038/sj.cr.7310149.

5. Hsu C, Shi J, Yuan C, et al. Recognition of histone acetylation by the GAS41 YEATS domain promotes H2A.Z deposition in non-small cell lung cancer. *Genes Dev*. 2018;32(1):58–69. doi: 10.1101/gad.303784.117.

6. Friedman MJ, Wagner T, Lee H, Rosenfeld MG, Oh S. Enhancer-promoter specificity in gene transcription: Molecular mechanisms and disease associations. *Exp Mol Med*. 2024;56(4):772–787. doi: 10.1038/s12276-024-01233-y.

7. Kim Y, Yu J, Lee S, et al. Cell adhesion status-dependent histone acetylation is regulated through intracellular contractility-related signaling activities. *J Biol Chem*. 2005;280(31):28357–28364. doi: 10.1074/jbc.M412608200.

8. Dahlin JL, Nelson KM, Strasser JM, et al. Assay interference and off-target liabilities of reported histone acetyltransferase inhibitors. *Nat Commun*. 2017;8(1):1527–3. doi: 10.1038/s41467-017-01657-3.

9. Shimazu T, Hirschey MD, Newman J, et al. Suppression of oxidative stress by beta-hydroxybutyrate, an endogenous histone deacetylase inhibitor. *Science*. 2013;339(6116):211–214. doi: 10.1126/science.1227166.

10. Cai L, Sutter BM, Li B, Tu BP. Acetyl-CoA induces cell growth and proliferation by promoting the acetylation of histones at growth genes. *Mol Cell*. 2011;42(4):426–437. doi: 10.1016/j.molcel.2011.05.004.

11. Fullgrabe J, Hajji N, Joseph B. Cracking the death code: Apoptosis-related histone modifications. *Cell Death Differ*. 2010;17(8):1238–1243. doi: 10.1038/cdd.2010.58.

12. Cheung WL, Ajiro K, Samejima K, et al. Apoptotic phosphorylation of histone H2B is mediated by mammalian sterile twenty kinase. *Cell*. 2003;113(4):507–517. doi: 10.1016/s0092-8674(03)00355-6.

13. Shi W, Cassmann TJ, Bhagwate AV, Hitosugi T, Ip WKE. Lactic acid induces transcriptional repression of macrophage inflammatory response via histone acetylation. *Cell Rep*. 2024;43(2):113746. doi: 10.1016/j.celrep.2024.113746.

14. Barnes PJ, Adcock IM, Ito K. Histone acetylation and deacetylation: Importance in inflammatory lung diseases. *Eur Respir J*. 2005;25(3):552–563. doi: 10.1183/09031936.05.00117504.

15. Yang X, Seto E. HATs and HDACs: From structure, function and regulation to novel strategies for therapy and prevention. *Oncogene*. 2007;26(37):5310–5318. doi: 10.1038/sj.onc.1210599.

16. Turgeon N, Blais M, Gagne J, et al. HDAC1 and HDAC2 restrain the intestinal inflammatory response by regulating intestinal epithelial cell differentiation. *PLoS One*. 2013;8(9):e73785. doi: 10.1371/journal.pone.0073785.

17. Zhang F, Qi L, Feng Q, et al. HIPK2 phosphorylates HDAC3 for NF-kappaB acetylation to ameliorate colitis-associated colorectal carcinoma and sepsis. *Proc Natl Acad Sci U S A*. 2021;118(28):e2021798118. doi: 10.1073/pnas.2021798118. doi: 10.1073/pnas.2021798118.

18. Aghdassi A, Sendler M, Guenther A, et al. Recruitment of histone deacetylases HDAC1 and HDAC2 by the transcriptional repressor ZEB1 downregulates E-cadherin expression in pancreatic cancer. *Gut*. 2012;61(3):439–448. doi: 10.1136/gutjnl-2011-300060.

19. Lu X, Fong K, Gritsina G, et al. HOXB13 suppresses de novo lipogenesis through HDAC3-mediated epigenetic reprogramming in prostate cancer. *Nat Genet*. 2022;54(5):670–683. doi: 10.1038/s41588-022-01045-8.

20. Wu S, Hashimoto-Hill S, Woo V, et al. Microbiota-derived metabolite promotes HDAC3 activity in the gut. *Nature*. 2020;586(7827):108–112. doi: 10.1038/s41586-020-2604-2.

21. Lu X, Cao X, Zhu Y, et al. Histone deacetylase 3 promotes liver regeneration and liver cancer cells proliferation through signal transducer and activator of transcription 3 signaling pathway. *Cell Death Dis*. 2018;9(3):398–x. doi: 10.1038/s41419-018-0428-x.

22. Gupta M, Han JJ, Stenson M, Wellik L, Witzig TE. Regulation of STAT3 by histone deacetylase-3 in diffuse large B-cell lymphoma: Implications for therapy. *Leukemia*. 2012;26(6):1356–1364. doi: 10.1038/leu.2011.340.

23. Sei, Yoshitatsu, et al. "A hereditary form of small intestinal carcinoid associated with a germline mutation in inositol polyphosphate multikinase." *Gastroenterology* 149.1 (2015): 67-78.doi: 10.1053/j.gastro.2015.04.008

24. Bukowinski A, Chang B, Reid JM, et al. A phase 1 study of entinostat in children and adolescents with recurrent or refractory solid tumors, including CNS tumors: Trial ADVL1513, pediatric early phase-clinical trial network (PEP-CTN). *Pediatr Blood Cancer*. 2021;68(4):e28892. doi: 10.1002/pbc.28892.

25. Watson PJ, Fairall L, Santos GM, Schwabe JWR. Structure of HDAC3 bound to co-repressor and inositol tetraphosphate. *Nature*. 2012;481(7381):335–340. doi: 10.1038/nature10728.

26. Sun Z, Feng D, Fang B, et al. Deacetylase-independent function of HDAC3 in transcription and metabolism requires nuclear receptor corepressor. *Mol Cell*. 2013;52(6):769–782. doi: 10.1016/j.molcel.2013.10.022.

27. Watson PJ, Millard CJ, Riley AM, et al. Insights into the activation mechanism of class I HDAC complexes by inositol phosphates. *Nat Commun*. 2016;7:11262. doi: 10.1038/ncomms11262.

28. Guha P, Tyagi R, Chowdhury S, et al. IPMK mediates activation of ULK signaling and transcriptional regulation of autophagy linked to liver inflammation and regeneration. *Cell Rep*. 2019;26(10):2692–2703.e7. doi: 10.1016/j.celrep.2019.02.013.

29. Cohen NN, Werbitt W. Inflammatory disease of the colon with fistulization to the posterior membranous urethra. *Am J Proctol*. 1975;26(1):59–62.doi: 10.1053/j.gastro.2015.04.008

30. Reilly L, Semenza ER, Koshkaryan G, et al. Loss of PI3k activity of inositol polyphosphate multikinase impairs PDK1-mediated AKT activation, cell migration, and intestinal homeostasis. *iScience*. 2023;26(5):106623. doi: 10.1016/j.isci.2023.106623.

31. Ge Y, Zadeh M, Mohamadzadeh M. Dissociation and flow cytometric isolation of murine intestinal epithelial cells for multi-omic profiling. *STAR Protoc*. 2023;4(1):101936. doi: 10.1016/j.xpro.2022.101936.

32. Vandenbroucke RE, Dejonckheere E, Van Hauwermeiren F, et al. Matrix metalloproteinase 13 modulates intestinal epithelial barrier integrity in inflammatory diseases by activating TNF. *EMBO Mol Med*. 2013;5(7):1000–1016. doi: 10.1002/emmm.201202100.

33. Odenwald MA, Turner JR. The intestinal epithelial barrier: A therapeutic target? *Nat Rev Gastroenterol Hepatol*. 2017;14(1):9–21. doi: 10.1038/nrgastro.2016.169.

34. Baugh MD, Perry MJ, Hollander AP, et al. Matrix metalloproteinase levels are elevated in inflammatory bowel disease. *Gastroenterology*. 1999;117(4):814–822. doi: 10.1016/s0016-5085(99)70339-2.

35. Millard CJ, Watson PJ, Celardo I, et al. Class I HDACs share a common mechanism of regulation by inositol phosphates. *Mol Cell*. 2013;51(1):57–67. doi: 10.1016/j.molcel.2013.05.020.

36. Bein A, Lubetzky R, Mandel D, Schwartz B. TIMP-1 inhibition of occludin degradation in caco-2 intestinal cells: A potential protective role in necrotizing enterocolitis. *Pediatr Res*. 2015;77(5):649–655. doi: 10.1038/pr.2015.26.

37. Wu S, Hashimoto-Hill S, Woo V, et al. Microbiota-derived metabolite promotes HDAC3 activity in the gut. *Nature*. 2020;586(7827):108–112. doi: 10.1038/s41586-020-2604-2.

38. Grases F, Simonet BM, Vucenik I, et al. Absorption and excretion of orally administered inositol hexaphosphate (IP(6) or phytate) in humans. *Biofactors*. 2001;15(1):53–61. doi: 10.1002/biof.5520150105.

39. Yilmaz OH, Katajisto P, Lamming DW, et al. mTORC1 in the paneth cell niche couples intestinal stem-cell function to calorie intake. *Nature*. 2012;486(7404):490–495. doi: 10.1038/nature11163.

40. Ghoroghi S, Mary B, Larnicol A, et al. Ral GTPases promote breast cancer metastasis by controlling biogenesis and organ targeting of exosomes. *Elife*. 2021;10:10.7554/eLife.61539. doi: 10.7554/eLife.61539.

41. Khan IZ, Del Guzzo CA, Shao A, et al. The CD200-CD200R axis promotes squamous cell carcinoma metastasis via regulation of cathepsin K. *Cancer Res*. 2021;81(19):5021–5032. doi: 10.1158/0008-5472.CAN-20-3251.

42. Kim W, Kim E, Min H, et al. Inositol polyphosphates promote T cell-independent humoral immunity via the regulation of bruton's tyrosine kinase. *Proc Natl Acad Sci U S A*. 2019;116(26):12952–12957. doi: 10.1073/pnas.1821552116.

43.Pavlovic, I., Thakor, D. T., Bigler, L., Wilson, M. S., Laha, D., Schaaf, G., ... & Jessen, H. J. (2015). Prometabolites of 5-Diphospho-myo-inositol Pentakisphosphate. *Angewandte Chemie*, *127*(33), 9758-9762.doi.org/10.1002/anie.201503094

44. Justus CR, Marie MA, Sanderlin EJ, Yang LV. Transwell in vitro cell migration and invasion assays. *Methods Mol Biol*. 2023;2644:349–359. doi: 10.1007/978-1-0716-3052-5_22.

45. Alenghat T, Osborne LC, Saenz SA, et al. Histone deacetylase 3 coordinates commensal-bacteria-dependent intestinal homeostasis. *Nature*. 2013;504(7478):153–157. doi: 10.1038/nature12687.

46. Wilson MS, Jessen HJ, Saiardi A. The inositol hexakisphosphate kinases IP6K1 and -2 regulate human cellular phosphate homeostasis, including XPR1-mediated phosphate export. *J Biol Chem*. 2019;294(30):11597–11608. doi: 10.1074/jbc.RA119.007848.

47. Fonseca TL, Garcia T, Fernandes GW, Nair TM, Bianco AC. Neonatal thyroxine activation modifies epigenetic programming of the liver. *Nat Commun*. 2021;12(1):4446–8. doi: 10.1038/s41467-021-24748-8.

48. Massimino L, Lamparelli LA, Houshyar Y, et al. The inflammatory bowel disease transcriptome and metatranscriptome meta-analysis (IBD TaMMA) framework. *Nat Comput Sci*. 2021;1(8):511–515. doi: 10.1038/s43588-021-00114-y.

46. Zhou Y, Zhou B, Pache L, et al. Metascape provides a biologist-oriented resource for the analysis of systems-level datasets. *Nat Commun*. 2019;10(1):1523–6. doi: 10.1038/s41467-019-09234-6.

47. Khan IZ, Del Guzzo CA, Shao A, et al. The CD200-CD200R axis promotes squamous cell carcinoma metastasis via regulation of cathepsin K. *Cancer Res*. 2021;81(19):5021–5032. doi: 10.1158/0008-5472.CAN-20-3251.

48. Kim W, Kim E, Min H, et al. Inositol polyphosphates promote T cell-independent humoral immunity via the regulation of bruton's tyrosine kinase. *Proc Natl Acad Sci U S A*. 2019;116(26):12952–12957. doi: 10.1073/pnas.1821552116.

49.Pavlovic, I., Thakor, D. T., Bigler, L., Wilson, M. S., Laha, D., Schaaf, G., ... & Jessen, H. J. (2015). Prometabolites of 5-Diphospho-myo-inositol Pentakisphosphate. *Angewandte Chemie*, *127*(33), 9758-9762.doi.org/10.1002/anie.201503094

Figure Legends

Figure 1: *Inositol phosphate multi kinase (IPMK) deletion* diminishes HDAC1 and HDAC3 activity in HCT116 cell line and mice models. (A) Schematic diagram of HDAC activity assay. Immunoprecipitation of selective HDACs from cell lysate followed by measuring HDAC activity fluorometrically after specific substrate reaction in a 96-well dark half area opaque microtiter plate. (B) HDAC1, HDAC2, HDAC3, and HDAC8 were immunoprecipitated from *IPMK-WT* (WT) and *IPMK-KO* (KO) HCT116 cells followed by evaluation of activity assay for the respective HDACs. HDAC1 and HDAC3 activity was markedly decreased in *IPMK-KO* (KO) HCT116 cells compared to *IPMK-WT* (WT) HCT 116 cells (n=12 and n=11 respectively). The activity of HDAC 2 and 8 in *IPMK-KO* (KO) HCT116 cells were comparable to *IPMK-WT* (WT) HCT116 cells (n=3). IgG was used as a negative control. Data has been presented as fold change compared with IgG. Results are representative of minimum three individual experiments. (***$p<0.0001$ vs WT, NS= not significant vs WT). (C) Immunoblot analysis of HDAC1, HDAC2, HDAC3, and HDAC8 from the whole cell lysate isolated from *IPMK-WT* (WT) and *IPMK-KO* (KO) HCT 116 cells demonstrate comparable amounts of protein levels in the lists from both genotypes. Actin was used as a loading control. The result was representative of three individual experiments, (n=3). (D) $CD45^-/CD31^-/TER\text{-}119^-/EpCam^+$ intestinal epithelial cells were isolated from $IPMK^{F/F}$ and $IPMK^{\Delta IEC}$ mice through FACS purification. Immunoblot analysis shows at protein level, IPMK was diminished in intestinal epithelial cell lysate from $IPMK^{\Delta IEC}$ compared to $IPMK^{F/F}$. HDAC1/3 protein level was comparable in both genotypes. Actin was used as a loading control. The result was representative of three

individual experiments, (n=3). (E) HDAC1/3 activity was diminished in Intestinal epithelial cells isolated from IPMK$^{\Delta IEC}$ compared with IPMK$^{F/F}$. HDAC1 and HDAC3 were separately immunoprecipitated from FACS purified intestinal epithelial cells followed by activity assay. Results are representative of three independent experiments, (n=3, ***p<0.0001). (F) CD45^{-}/CD31^{-}/TER-119^{-}/EpCam^{+} intestinal epithelial cells were isolated from *IPMK* Floxed (IPMK$^{F/F}$) and "tamoxifen induced" intestinal epithelial cell specific *IPMK* deleted (IPMK$^{\Delta Tam\text{-}IEC}$) mice through FACS purification. Immunoblot analysis showed at protein level IPMK was diminished in whole intestinal epithelial cell lysate from IPMK$^{\Delta Tam\text{-}IEC}$ compared to IPMK$^{F/F}$. HDAC1/3 protein level was comparable in both genotypes. Actin was used as a loading control. The result was representative of three individual experiments, (n=3). (G) HDAC1/3 activity was diminished in IPMK$^{\Delta Tam\text{-}IEC}$ compared with IPMK$^{F/F}$. Results are representative of three independent experiments. (n=3, ***p<0.0001).

Figure 2: Kinase activity of IPMK is essential for activating HDAC1 and HDAC3

(A) Pictorial representation demonstrates the function of IPMK in the higher-order inositol phosphate (HOIP) pathway. (B, C) *IPMK*-KO (KO) HCT116 cells transiently overexpressed with *myc-control*, *IPMK-WT*-myc*,* and *IPMK-KSA*-myc plasmid. HDAC1 and HDAC3 were immunoprecipitated from the lysates isolated from *myc-control*, *IPMK-WT*-myc*,* and *IPMK-KSA*-myc overexpressed cells, followed by HDAC1/3 activity assay. Results demonstrated that *myc-control* and *IPMK-KSA*-myc *were* unable to rescue HDAC1/3 activity as compared with *IPMK-WT*-myc*.* Results were representative of three independent experiments (n=3,***p<0.001). (D) Immunoblot analysis against anti-myc antibody confirmed the efficacy of transient transfection. Actin is used as the loading control. The result was representative of three individual experiments (n=3). Next, to analyze the role of InsP6 in activating HDAC1/3 activity *in vitro*, endogenous HDAC1 and HDAC3 were immunopurified from *IPMK-WT* HCT116 (WT) and *IPMK-KO* HCT 116 (KO) cells followed by dose-dependent (0.001 μM, 0.01 μM, 0.1 μM, 0.5 μM, 1 μM, 5 μM and 10 μM) *in vitro* InsP6 treatment. The result was representative of three individual experiments (n=3, ***p<0.0001, NS= Non significant). (G, H) To analyze the impact of other HOIPs and PIP3 in HDAC1 and HDAC3 activity, endogenous HDAC1 and HDAC3 were immunopurified from *IPMK-WT* HCT116 (WT) and *IPMK-KO* HCT 116 (KO) cells followed by *in vitro* 10μM treatment with PIP3, InsP3, Ins (1,3,4,5)P4 and 1μM of Ins (1,4,5,6)P4, InsP5 and InsP6. The result was representative of three individual experiments (n=3, ***p<0.0001, NS= Non significant).

Figure 3: IPMK directly binds with HDAC1 and HDAC3

(A, B) To analyze endogenous binding between HDAC1 and HDAC3 with IPMK, HDAC1 and HDAC3 immunoprecipitated from whole cell lysate isolated from *IPMK-WT* HCT116 (WT) and *IPMK-KO* HCT 116 (KO) cells followed by immunoblotting with anti-IPMK antibody showed endogenous IPMK binds with HDAC1 and HDAC3. IgG was used as a negative control. Immunoblotting against anti-HDAC1, anti-HDAC3, and anti-IPMK antibodies from the lysates isolated from *IPMK-WT* HCT116 (WT) and *IPMK-KO* HCT 116 (KO) cells were used as input control while actin was used as the loading control. The result was representative of three individual experiments (n=3).

Figure 4: *IPMK* deletion increases histone acetylation.

In (A) and (B), western blot analysis demonstrated that histone acetylation increased in *IPMK-KO* -HCT 116 cells (KO) compared to the *IPMK-WT* HCT 116 cells (WT). *IPMK-WT HCT* 116 (WT) cells were treated overnight with 5μM of HDAC1/3 specific inhibitor Entinostat as a positive control. (A) *IPMK* deletion specifically increased acetylated H3K9, 18, and 27 and was comparable to the entinostat. (B) *IPMK* deletion selectively increased acetylated H4k16 acetylation and was comparable to entinostat. The data represents 3 experimental replicates (n=3). The loadings H3 or H4 are re-probed after stripping respective acetylated histone.

Figure 5: Deletion of *IPMK* changes global transcriptomics in cell lines and mice models

(A) Volcano plot (Log 10[*FDR*] vs. Log 2[Fold change]) displays differentially expressed genes after *IPMK* deletion in HCT116 cells (*IPMK-KO*) as compared to WT-HCT116 cells (*IPMK-WT*). Red dots represent gene expression that was upregulated, while blue dots represent gene expression that was downregulated in *IPMK* KO cells. Y-axis denotes –Log10 FDR Value, while the X-axis denotes the Log2 fold change value. The result was representative of three individual experiments (n=3). (B) The Pearson correlation coefficient analysis revealed a strong positive correlation between the two groups, with a correlation coefficient 0.90. Scatterplot represents all differentially expressed genes from *IPMK-KO* HCT 116 cells, or 5μM of HDAC1/3 specific inhibitor Entinostat treated *WT-IPMK* HCT116 cells. The values for the respective gene change were represented as Log2 fold changes, with the X-axis corresponding to *IPMK-KO* HCT 116 cells and the Y-axis representing 5μM Entinostat-treated *IPMK-WT* HCT 116 cells. The result was representative of three individual experiments (n=3). (C) The Venn diagram represented upregulated differentially expressed genes (DEGs) in *IPMK-KO* HCT 116 cells, and WT+Entinostat treated HCT-116 cells showed 2778 Genes (60.1%) overlap between both groups. We named these two groups overlapped genes IPMK-HDAC-OVERLAP-GENES (IHOG). (D) Venn diagram represented upregulated differentially expressed genes (DEGs) in *IPMK-KO* HCT 116 cells, WT+Entinostat treated HCT116 cells, and IPMK $^{\Delta IEC}$ mice derived intestinal epithelial cells showed 250 genes overlapped between all three groups. (E) Pathway analysis of common genes between IHOG and IPMK $^{\Delta IEC}$ mice RNA

seq data. (F) Volcano plot (Log 10[*FDR*] vs. Log 2[Fold change]) displays differentially expressed genes in Crohn's disease patients from the Inflammatory Bowel Disease Transcriptome and Metatranscriptome Meta-Analysis (IBD TaMMA) database as compared with healthy individuals. Red dots represent gene expression upregulated in Crohn's patient ileum, while blue dots represent downregulated gene expression. The Y-axis denotes the –Log10 FDR Value, while the X-axis denotes the Log2 fold change value. The result represented an expression of various MMP genes high in Crohn's disease patient's ileum.

Figure 6: *IPMK* deletion markedly increases cell and gut permeability

(A) Schematic diagram of transwell cell permeability assay. (B) Transwell cell permeability assay showing *IPMK-WT* (WT) HCT116 cells do not exhibit cell permeability within 25-30 min of FITC-Dextran treatment while *IPMK-KO* HCT116 cells (KO) shows cell permeability after 5 min, reaching maximum at 25 min time point. 4 kDa-FITC-Dextran was added to the top well at 25 mg/ml, at 37°C, and fluorescence was measured after 0 min, 5 min, 10 min, 15 min, 20 min, 25 min, 30 min, 45 min, and 1 hr by using a Spectramax iD5 plate reader (Molecular Devices, (excitation 485 nm/emission 535 nm). Values were represented as a fold change with respect to untreated sets. Results were representative of three individual experiments (n=3, *p<0.001). (C) FITC-Dextran Transwell assay showing 5μM HDAC1/3 specific inhibitor Entinostat treatment in *IPMK-WT* (WT) HCT116 cells increase cell permeability while either 10 μM Pan-MMPs inhibitor Ilomastat or 50 μM cell permeable InsP6 treatment in *IPMK-KO* HCT116 (KO) cells significantly rescued cell permeability. Values were represented as a fold change with respect to untreated sets. Results were representative of three individual experiments (n=3, *p<0.001). (D) Pictorial representation demonstrates *in vivo* intestinal permeability assay. (E, F) Results indicated a significant increase in 4Kda FITC Dextran fluorescence in IPMK$^{\Delta IEC}$ or "tamoxifen-induced" *IPMK* deleted (IPMK$^{\Delta Tam\text{-}IEC}$) mice serum. Values were represented as a fold change with respect to PBS-treated mice (***p<0.001).

Extended Figure 1: Generation of Inositol multi-kinase (*IPMK*) deleted HCT 116 cells and analysis of IPMK deletion diminish HDAC1/3 activity in MEF cell lines. (A) The schematic diagram represents the CRISPR deleted *IPMK* KO HCT 116 cell line generation procedure. (B) Western blot analysis of the lysates shows complete loss of IPMK protein in three *IPMK-KO* clones (E05, A11, B09) as compared to lysate isolated from *IPMK-WT* (WT) HCT116 cells. HDAC1 and 3 protein levels were comparable in all genotypes. Actin was used as a loading control. Results were representative of three individual experiments (n=3). (C) HDAC1 and HDAC3 activity were maximum diminished in IPMK-*KO* B09 clone compared with *IPMK-WT.* HDAC1 and HDAC3 were immunoprecipitated from *IPMK-WT* (WT) and three *IPMK-KO* clones (E05, A11, B09) followed by activity assay. Results were representative of three independent experiments (n=3, ***p<0.0001). (D) HDAC1, HDAC2, HDAC3, and HDAC8 were immunoprecipitated from *IPMK-WT* (WT) and *IPMK-KO* (KO) MEF cells followed by evaluation of activity assay for the respective HDACs. HDAC1 and HDAC3 activity was markedly decreased in *IPMK-KO* (KO) MEF cells compared to *IPMK-WT* (WT) MEF cells (n=4). The activity of HDAC 2 and 8 in *IPMK-KO* (KO) MEF cells was comparable to *IPMK-WT* (WT) MEF cells (n=3). IgG was used as a negative control. Data has been presented as fold change compared with IgG. Results are representative of three individual experiments (***p<0.0001, NS=not significant). (E) Immunoblot analysis of HDAC1, HDAC2, HDAC3, and HDAC8 from the whole cell lysate isolated from *IPMK-WT* (WT) and *IPMK-KO* (KO) MEF cells demonstrate comparable amounts of protein levels in the lysates from both genotypes. Actin was used as a loading control. The result was representative of three individual experiments (n=3). (F) Pictorial representation of FACS based intestinal

epithelial cell purification procedure. (G) After isolation, intestinal cells were flow purified, followed by staining with APC-CD45, FITC-CD31, PE/Cy7-TER-119 , and PE-EpCAM. Dead cells were excluded using the Tail Cell Cycle Solution, propidium iodide (PI). $CD45^-$ /$CD31^-$/$TER\text{-}119^-$ /$EpCAM^+$ intestinal epithelial cells were sorted using a SONY SH800S Cell Sorter. (H) Western blot analysis showed the purity of EpCAM + intestinal epithelial cell population. Lysate was isolated from unsorted and sorted intestinal cells, followed by western blot against anti-CD31, anti-CD45, anti-TER-119, and anti-EpCam. Actin was used as a loading control. Analysis showed that the sorted cell population was devoid of CD31, CD45, and TER-119 cell population but positive for EpCam. Results were representative of three individual experiments (n=3).

Extended Figure 2: *IPMK* deletion reduced InsP5 and InsP6 production in HCT 116 cells.

(A) HPLC analysis of inositol phosphate level depicted *IPMK* deletion reduced InsP5 and InsP6 levels in HCT 116 cells. The blue line indicated *IPMK- WT* HCT116 cells, and the red line indicated *IPMK-KO* HCT cells.

Extended Figure 3: In mice models, intestinal epithelial cell-specific IPMK deletion increases histone acetylation. In (A-B), western blot analysis demonstrated that histone acetylation increased in intestine specific constitutive *IPMK* deletion ($IPMK_{\Delta IEC}$) (A) or "tamoxifen-induced" transient *IPMK* deletion ($IPMK_{\Delta Tam\text{-}IEC}$) mice (B) intestinal epithelial cells compared with $IPMK_{F/F}$. (C) p300 activity from *IPMK-KO* (KO) HCT116 cells was comparable to *IPMK-WT* (WT). p300 protein was immuno-precipitated from IPMK-*WT* (WT) and *IPMK-KO* (KO) cells, followed by histone acetyltransferase (HAT) activity assay *in vitro*. IgG had been used as a negative control. Data has been presented as fold change compared to IgG. The result was representative of three individual experiments (n=3, NS-not significant). Immunoblot analysis of p300, from the total lysate isolated from *IPMK-WT* (WT) and *IPMK-KO* (KO) cells, was represented as input control, while actin was used as loading control. The result was representative of three individual experiments. (n=3).

Extended Figure 4: Deletion of *IPMK* and treatment of Entinostat changes global Transcriptomics in cell lines and mice models

(A) Volcano plot (Log 10[*FDR*] vs. Log 2[Fold change]) displays differentially expressed genes in 5 μM HDAC1/3 specific inhibitor Entinostat treated WT HCT116 cells (*IPMK*-WT+ Entinostat (5 μM)) as compared to untreated WT-HCT116 cells (*IPMK-WT*). Red dots represent gene expression upregulated in Entinostat-treated cells, while blue dots represent downregulated gene expression. The Y-axis denotes –the Log10 FDR Value, while the X-axis denotes the Log2 fold change value. The result was representative of three individual experiments (n=3). (B) Venn diagram represented downregulated differentially expressed genes (DEGs) in *IPMK-KO* HCT 116 cells and 5μM *IPMK-WT* HCT116 cells showed 2448 Genes (65.8%) overlapped between both groups. (C) Volcano plot (Log 10[*FDR*] vs. Log 2[Fold change]) displays differentially expressed genes in $IPMK_{\Delta IEC}$ as compared with IPMK $^{F/F}$ mice. Red dots represent gene expression that was upregulated in $IPMK_{\Delta IEC}$, while blue dots represent gene expression that was downregulated. The Y-axis denotes –the Log10 FDR Value, while the X-axis denotes the Log2 fold change value. The result was representative of three individual experiments (n=3). (D) Venn diagram represented downregulated differentially expressed genes (DEGs) in *IPMK-KO* HCT 116 cells, 5μM Entinostat treated *IPMK-WT* HCT116 cells, and RNA-seq of intestinal epithelial cells from $IPMK_{\Delta IEC}$ mice showed 383 genes overlapped between three groups. Result was representative of three individual experiments (n=3).

Extended Figure 5: Cell population density was comparable in *IPMK-WT* and *IPMK-KO* in transwell assay.

(A) To analyze adherent cell population density, after transwell assay, cells containing inserts were stained with 0.2% crystal violet staining solution. After three times washed with PBS. After lysing cells in ethanol and Sodium citrate containing lysis buffer, absorbance of lysate was measured at 590 nm by using a Spectramax iD5 plate reader (Molecular Devices). Result depicted Cell population density was comparable in both genotype. (B) To analysis adherent cell population density, after transwell assay, cell containing inserts were stained with 1µg/ ml DAPI staining solution. After three times washed with PBS fluorescence was measured at 358/461 nm by using a Spectramax iD5 plate reader (Molecular Devices). Result depicted Cell population density was comparable in both genotypes. Values represented as a fold change in respected with blank insert. Results were representative of Results were representative of three individual experiments. (n=3, *p<0.001).

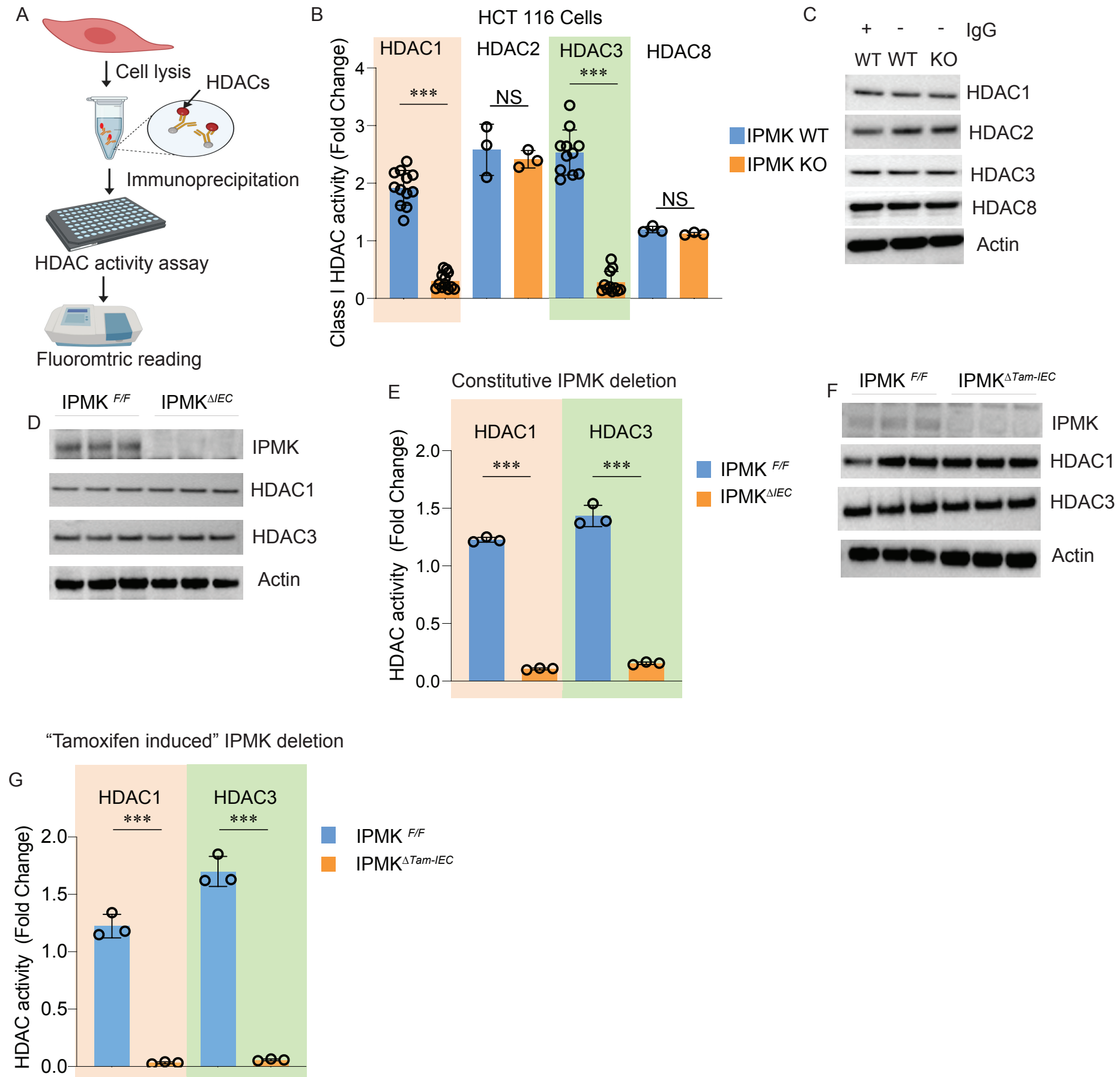
A
Cell lysis
HDACs
Immunoprecipitation
HDAC activity assay
Fluoromtric reading
B
HCT 116 Cells
HDAC1
HDAC2
HDAC3
HDAC8
***
NS
***
NS
Class I HDAC activity (Fold Change)
IPMK WT
IPMK KO
C
+ - - IgG
WT WT KO
HDAC1
HDAC2
HDAC3
HDAC8
Actin
D
IPMK F/F
IPMKΔIEC
IPMK
HDAC1
HDAC3
Actin
E
Constitutive IPMK deletion
HDAC1
HDAC3
***
***
HDAC activity (Fold Change)
IPMK F/F
IPMKΔIEC
F
IPMK F/F
IPMKΔTam-IEC
IPMK
HDAC1
HDAC3
Actin
"Tamoxifen induced" IPMK deletion
G
HDAC1
HDAC3
***
***
HDAC activity (Fold Change)
IPMK F/F
IPMKΔTam-IEC

Figure 1

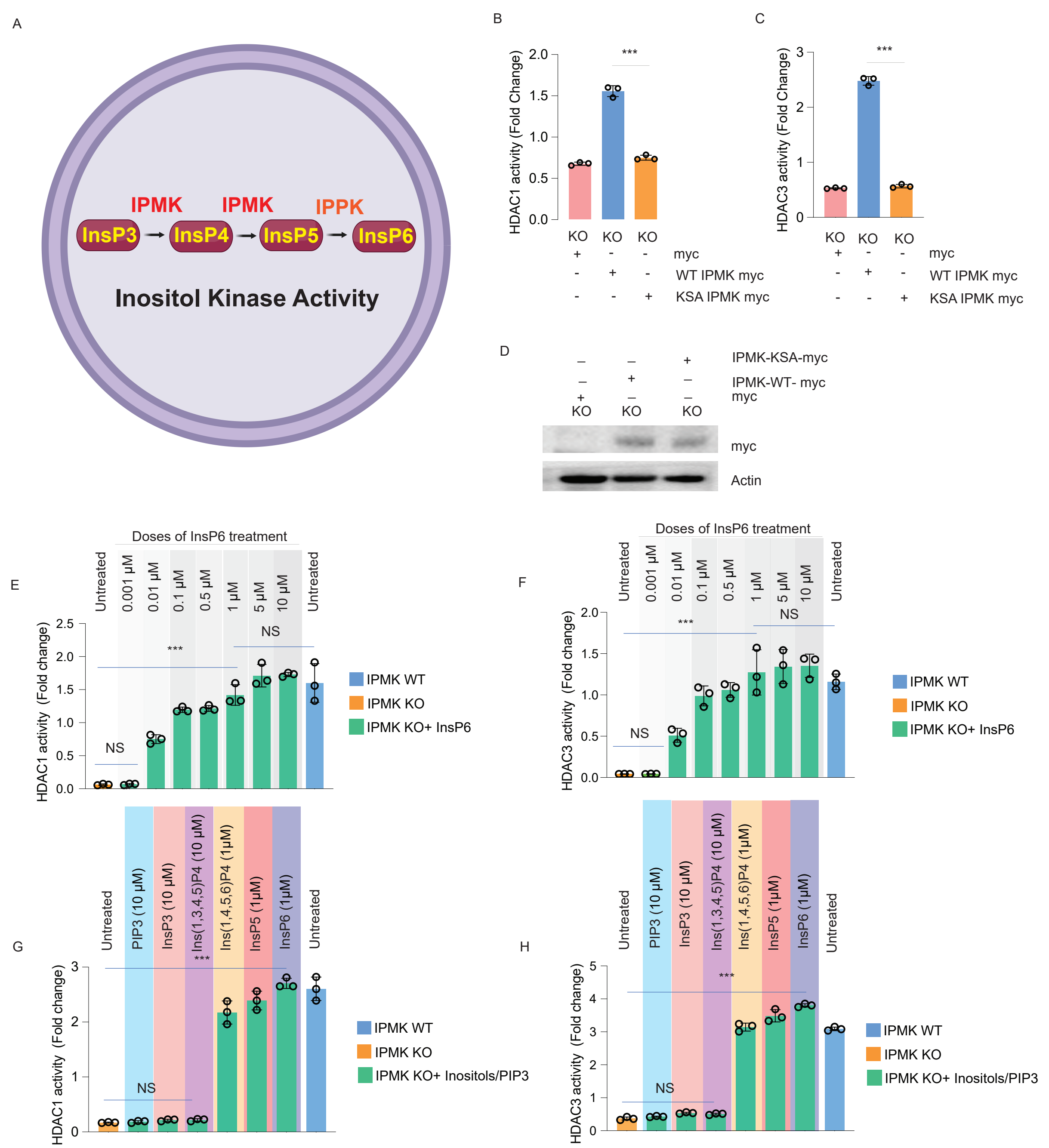
A
IPMK
IPMK
IPPK
InsP3
InsP4
InsP5
InsP6
Inositol Kinase Activity
B
HDAC1 activity (Fold Change)
***
KO KO KO
+ - - myc
- + - WT IPMK myc
- - + KSA IPMK myc
C
HDAC3 activity (Fold Change)
***
KO KO KO
+ - - myc
- + - WT IPMK myc
- - + KSA IPMK myc
D
IPMK-KSA-myc
IPMK-WT- myc
myc
KO KO KO
myc
Actin
E
Doses of InsP6 treatment
Untreated
0.001 μM
0.01 μM
0.1 μM
0.5 μM
1 μM
5 μM
10 μM
Untreated
HDAC1 activity (Fold change)
NS
***
IPMK WT
IPMK KO
IPMK KO+ InsP6
F
Doses of InsP6 treatment
HDAC3 activity (Fold change)
NS
***
IPMK WT
IPMK KO
IPMK KO+ InsP6
G
Untreated
PIP3 (10 μM)
InsP3 (10 μM)
Ins(1,3,4,5)P4 (10 μM)
Ins(1,4,5,6)P4 (1μM)
InsP5 (1μM)
InsP6 (1μM)
Untreated
HDAC1 activity (Fold change)
NS
***
IPMK WT
IPMK KO
IPMK KO+ Inositols/PIP3
H
HDAC3 activity (Fold change)
NS
***
IPMK WT
IPMK KO
IPMK KO+ Inositols/PIP3

Figure 2

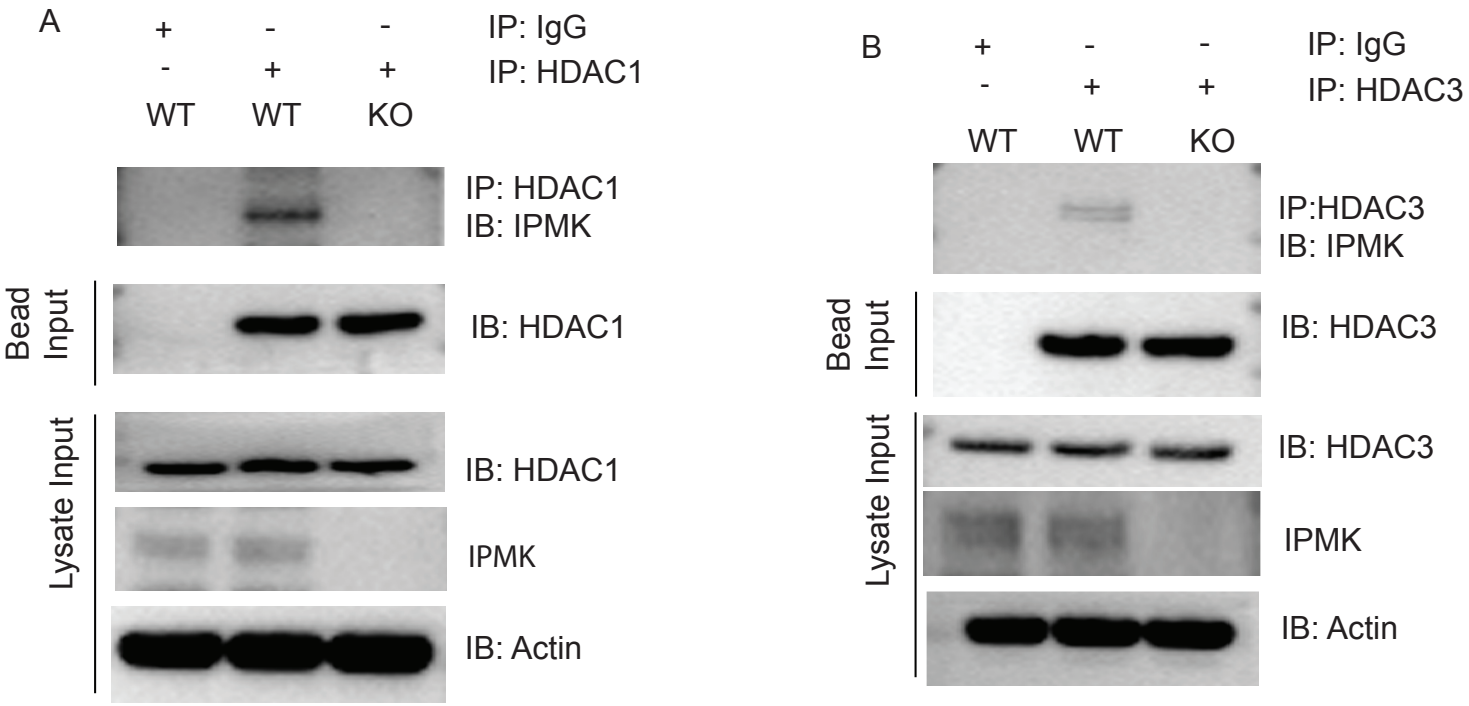
A
+ - -
IP: IgG
- + +
IP: HDAC1
WT WT KO
IP: HDAC1
IB: IPMK
Bead Input
IB: HDAC1
Lysate Input
IB: HDAC1
IPMK
IB: Actin
B
+ - -
IP: IgG
- + +
IP: HDAC3
WT WT KO
IP:HDAC3
IB: IPMK
Bead Input
IB: HDAC3
Lysate Input
IB: HDAC3
IPMK
IB: Actin

Figure 3

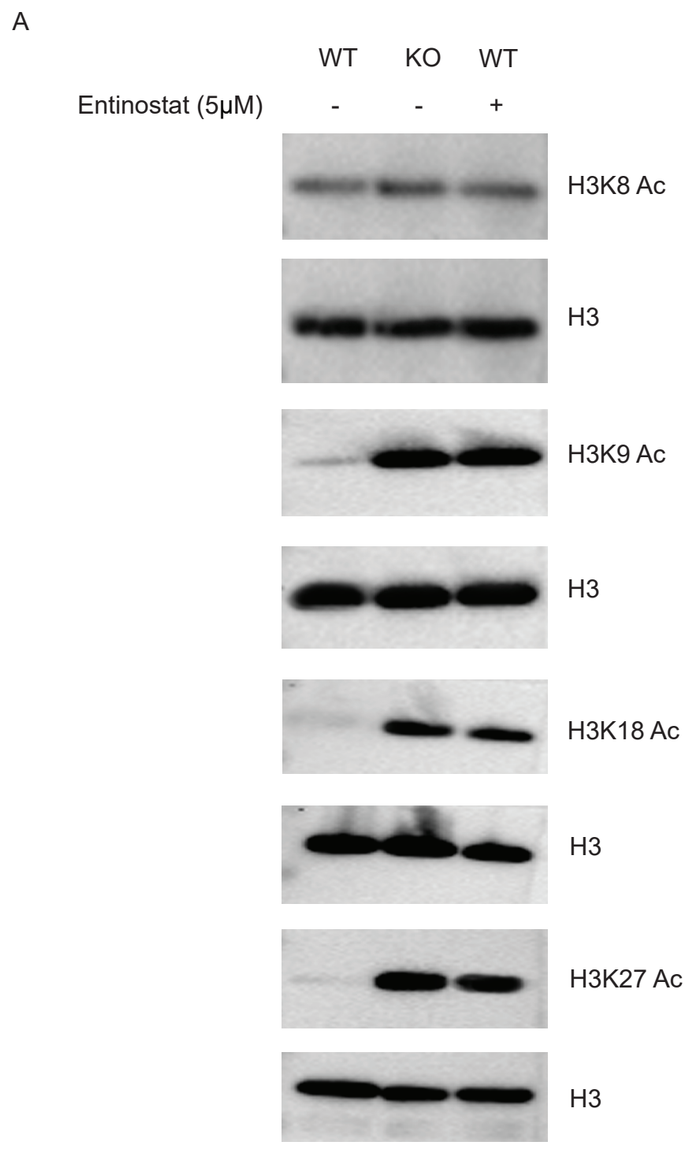
A
WT
KO
WT
Entinostat (5μM)
-
-
+
H3K8 Ac
H3
H3K9 Ac
H3
H3K18 Ac
H3
H3K27 Ac
H3

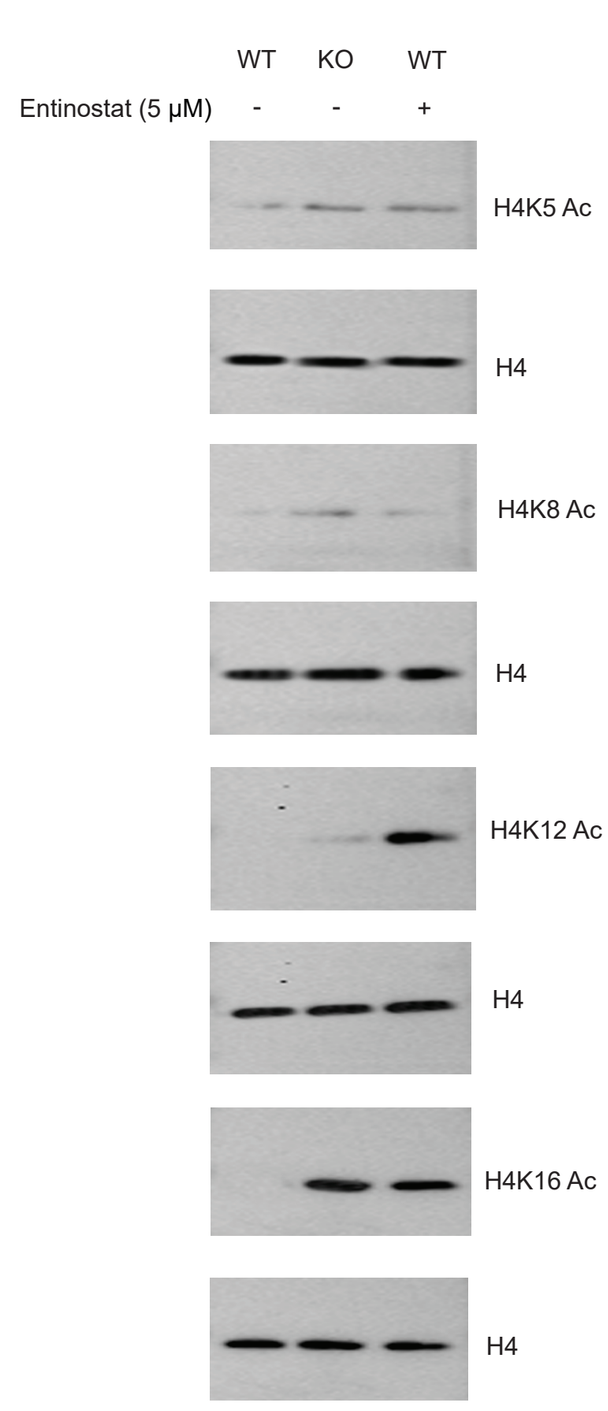
B
WT
KO
WT
Entinostat (5 μM)
-
-
+
H4K5 Ac
H4
H4K8 Ac
H4
H4K12 Ac
H4
H4K16 Ac
H4

Figure 4

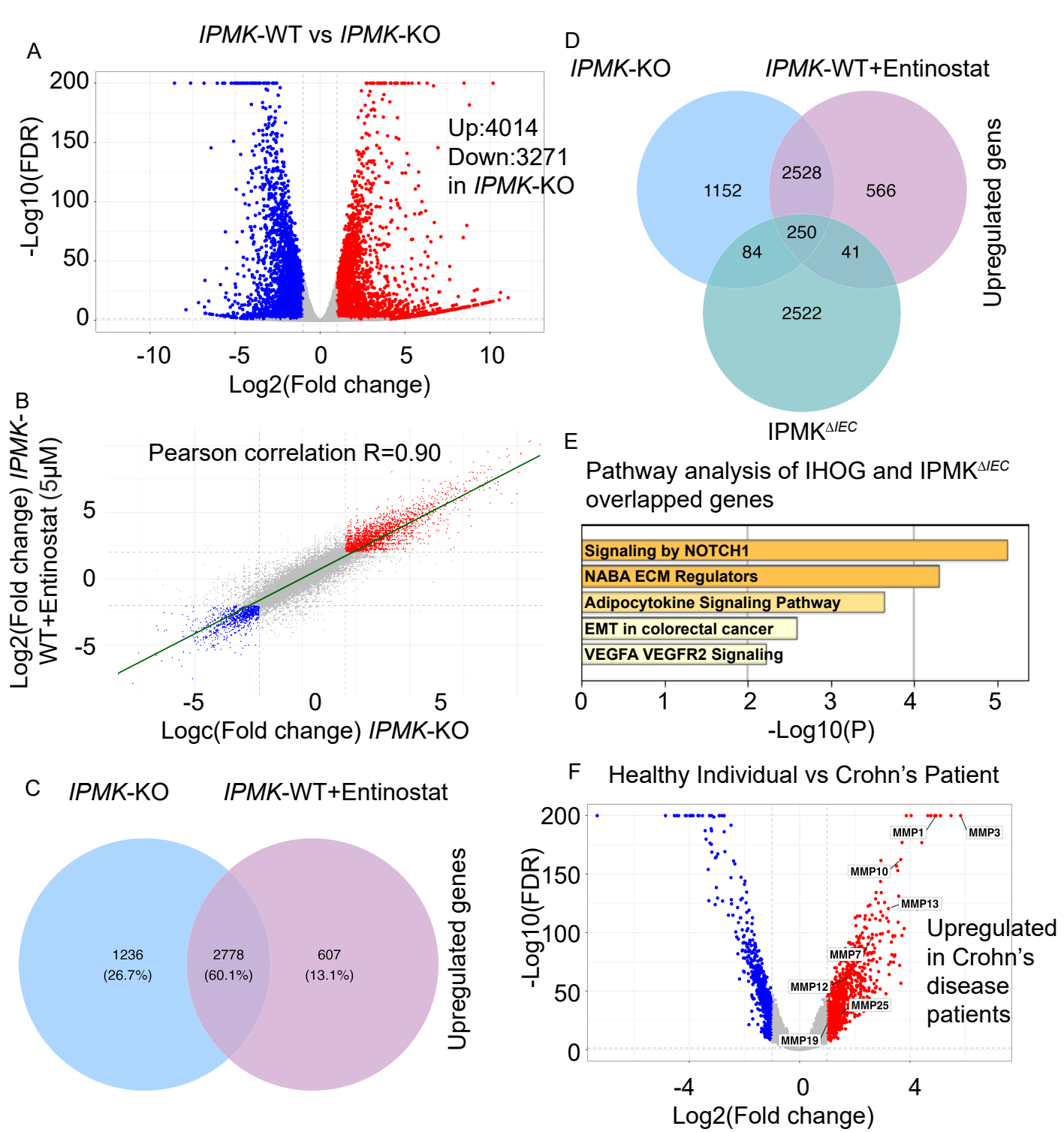
A
IPMK-WT vs IPMK-KO
-Log10(FDR)
Log2(Fold change)
Up:4014
Down:3271
in IPMK-KO
B
Pearson correlation R=0.90
Log2(Fold change) IPMK-WT+Entinostat (5μM)
Logc(Fold change) IPMK-KO
C
IPMK-KO
IPMK-WT+Entinostat
1236 (26.7%)
2778 (60.1%)
607 (13.1%)
Upregulated genes
D
IPMK-KO
IPMK-WT+Entinostat
IPMKΔIEC
1152
2528
566
250
84
41
2522
Upregulated gens
E
Pathway analysis of IHOG and IPMKΔIEC overlapped genes
Signaling by NOTCH1
NABA ECM Regulators
Adipocytokine Signaling Pathway
EMT in colorectal cancer
VEGFA VEGFR2 Signaling
-Log10(P)
F
Healthy Individual vs Crohn's Patient
-Log10(FDR)
Log2(Fold change)
MMP1
MMP3
MMP10
MMP13
MMP7
MMP12
MMP25
MMP19
Upregulated in Crohn's disease patients

Figure 5

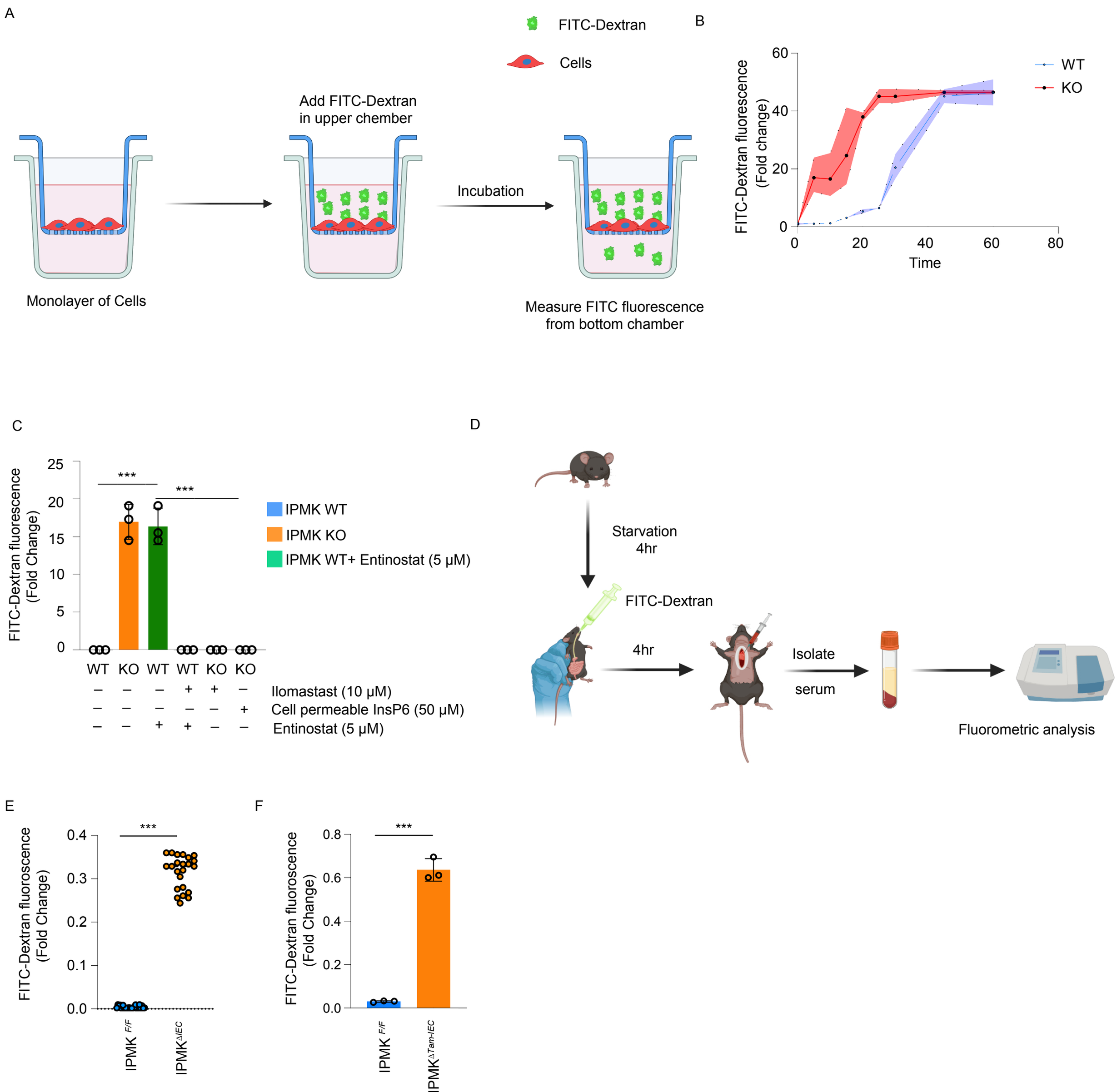
A
FITC-Dextran
Cells
Add FITC-Dextran
in upper chember
Incubation
Monolayer of Cells
Measure FITC fluorescence
from bottom chamber
B
FITC-Dextran fluorescence
(Fold change)
Time
WT
KO
C
FITC-Dextran fluorescence
(Fold Change)
IPMK WT
IPMK KO
IPMK WT+ Entinostat (5 μM)
WT KO WT WT KO KO
Ilomastast (10 μM)
Cell permeable InsP6 (50 μM)
Entinostat (5 μM)
D
Starvation
4hr
FITC-Dextran
4hr
Isolate
serum
Fluorometric analysis
E
FITC-Dextran fluorescence
(Fold Change)
IPMK F/F
IPMK ΔIEC
F
FITC-Dextran fluorescence
(Fold Change)
IPMK F/F
IPMK ΔTam-IEC

Figure 6

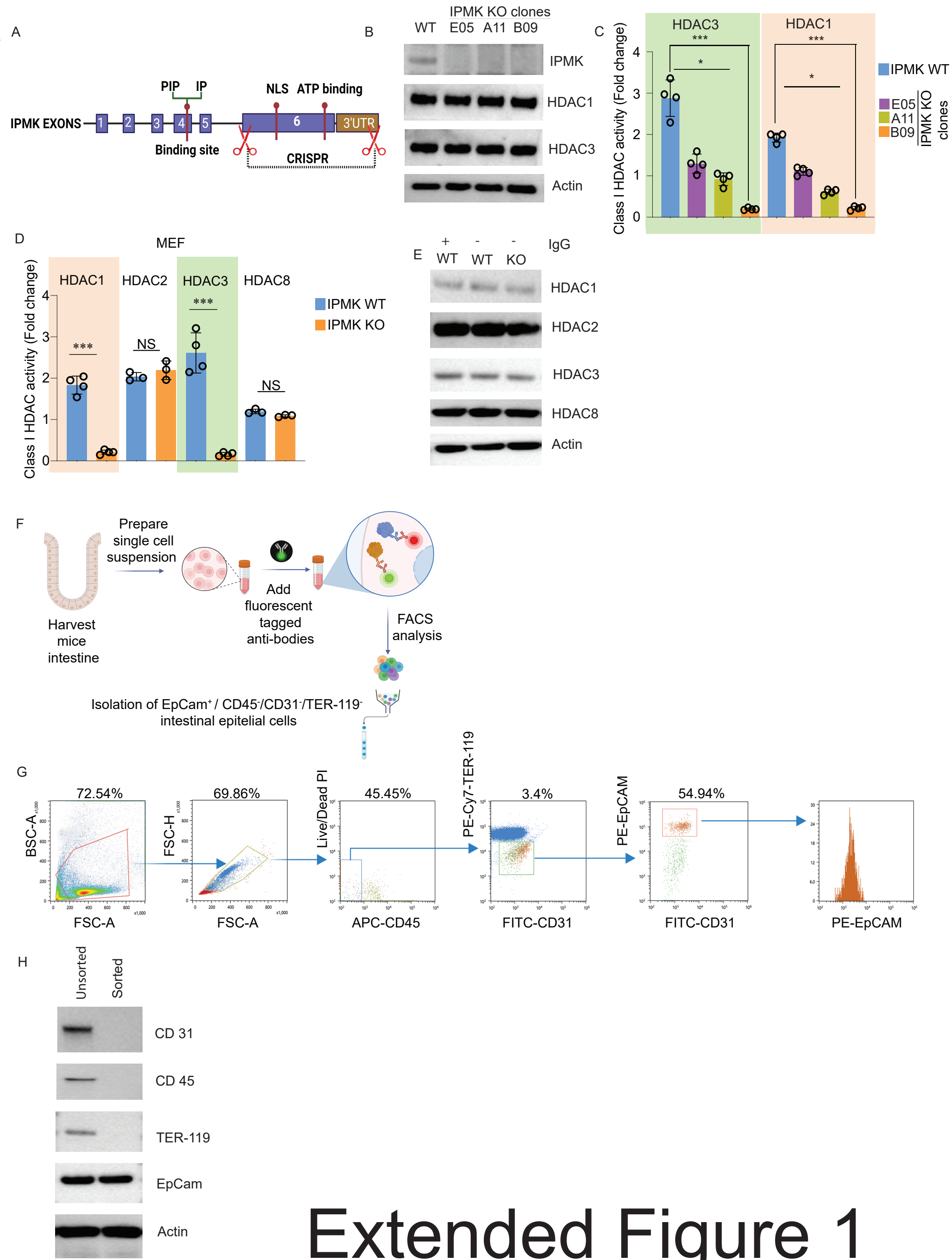

Extended Figure 1

A

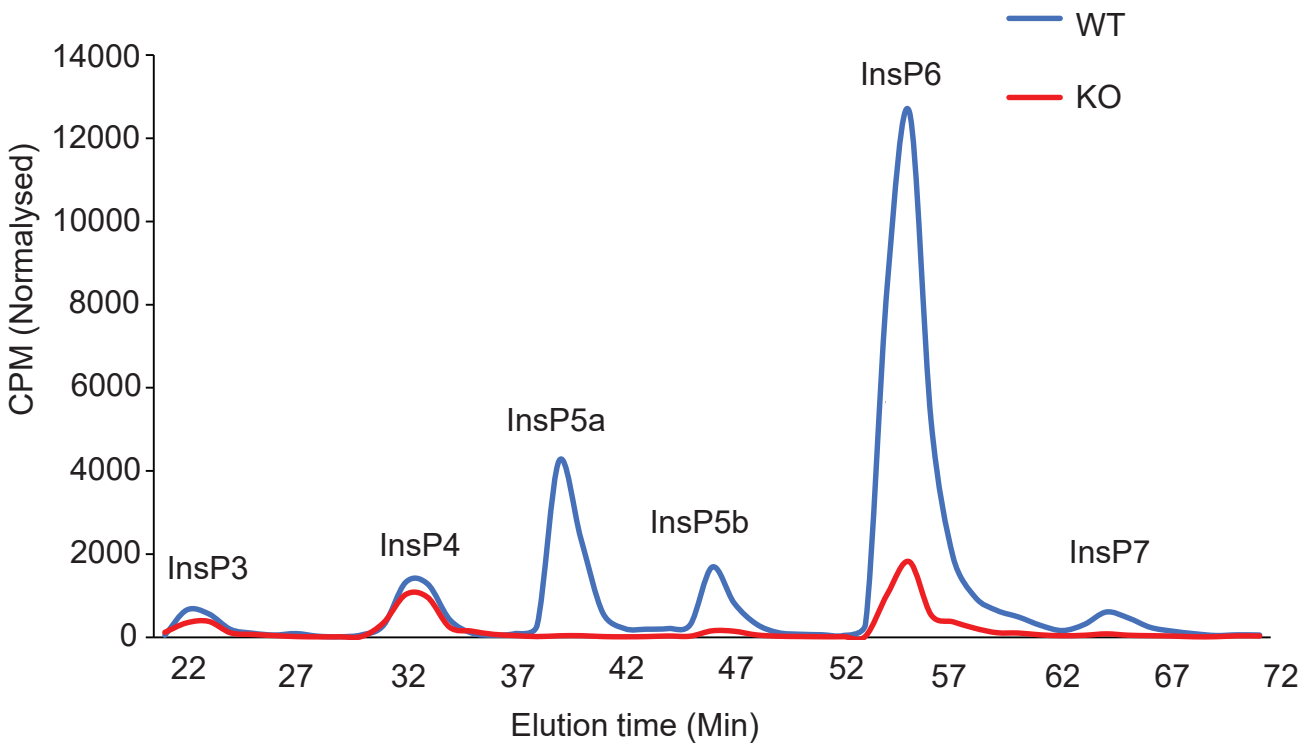

Extended Figure 2

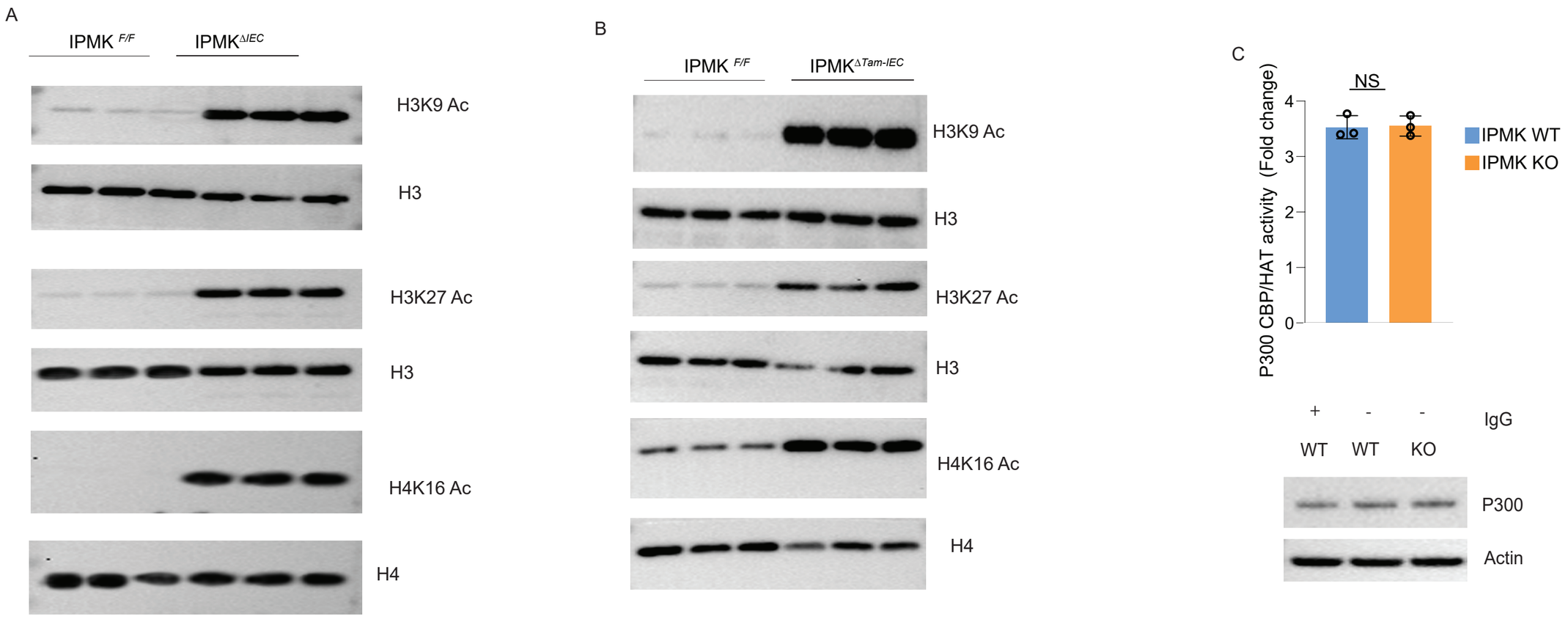

Extended Figure 3

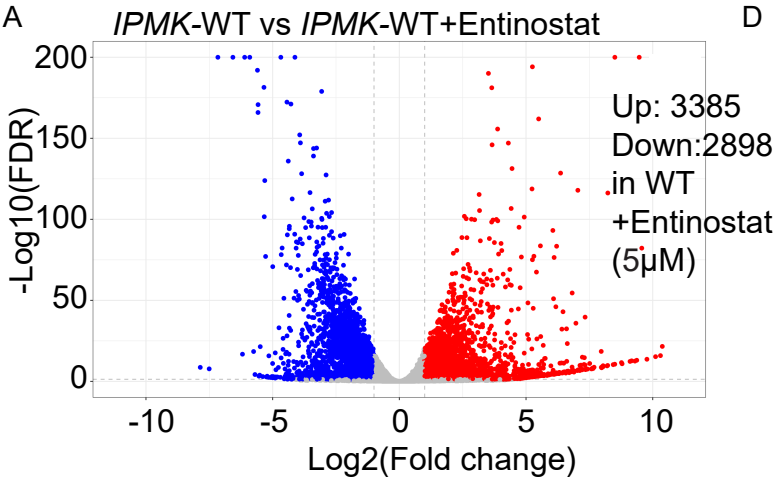

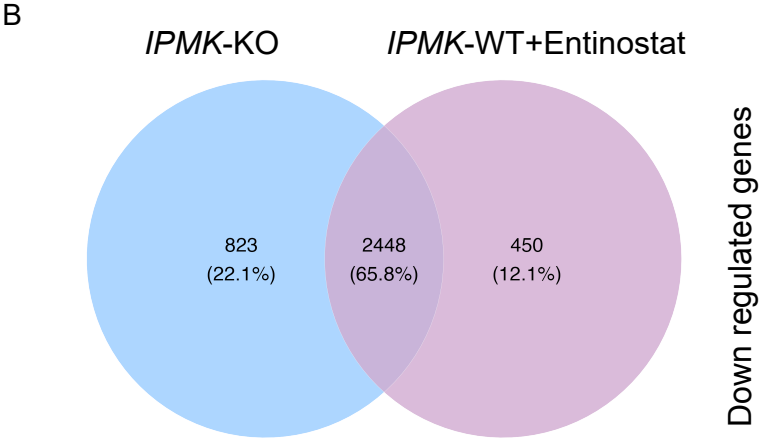

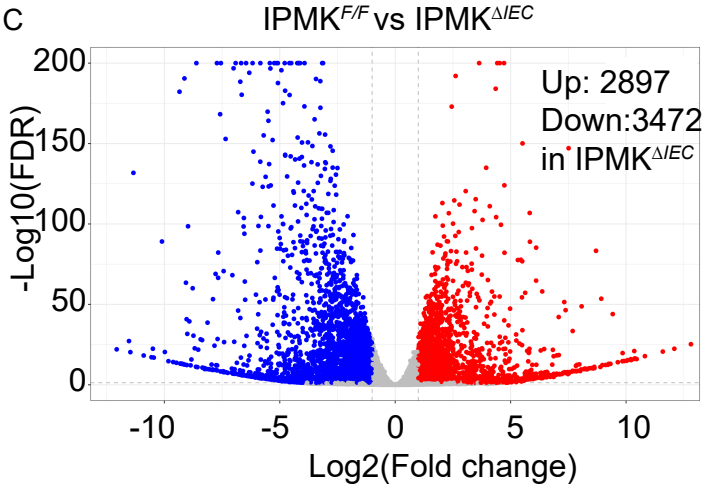

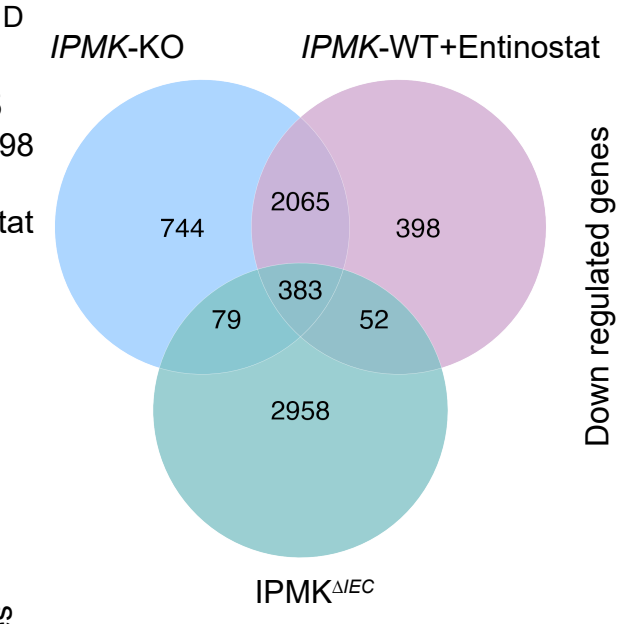

Extended Figure 4

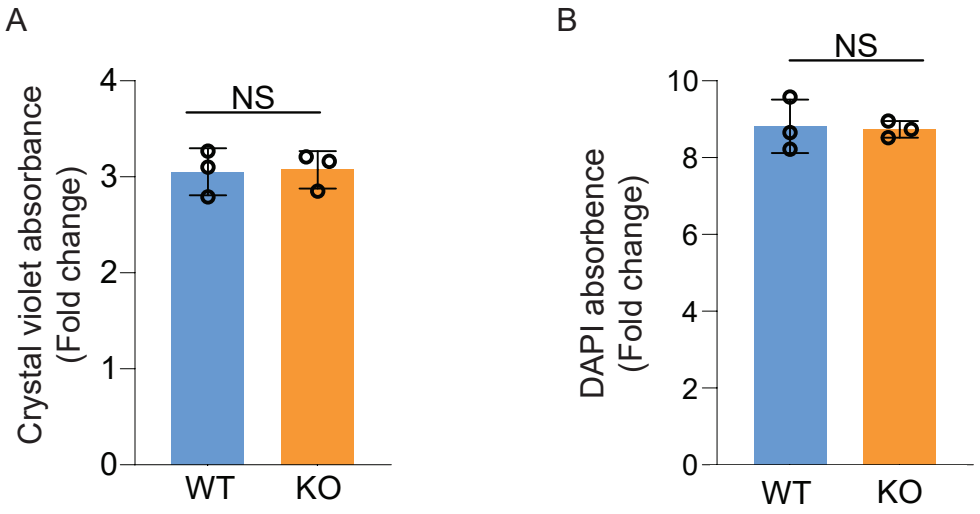

Extended Figure 5